Dynamic interaction of plates in an inhomogeneous transversely isotropic space weakened by a crack

A. Amiri-Hezaveh[a], **H. Moghaddasi**[b], **P. Karimi**[a], **M. Ostoja-Starzewski**[a,c]

[a] Department of Mechanical Science and Engineering, University of Illinois at Urbana-Champaign, Urbana, IL 61801, USA

[b] School of Civil and Environmental Engineering, University of New South Wales, Sydney, 2052, Australia

[c] Institute for Condensed Matter Theory and Beckman Institute, University of Illinois at Urbana-Champaign, Urbana, IL 61801, USA

Abstract: The problem of axisymmetric vibration of a flat thin rigid circular plate located inside a vertically exponentially graded, transversely isotropic material of infinite extent is addressed by means of a displacement potential method. The contact condition on one side of the foundation is assumed to be the perfect adhesion with the media but known to be faced by a penny-shaped crack at the other side as it occurs in anchors. The mixed boundary value problem is formulated with the aid of Hankel integral transforms and is written in the form of a set of singular integral equations. The analytical procedure for the special case of vertical movement of the rigid plate results in a closed form solution. The solution is pursued numerically for the general elastodynamic case. The physical quantities, such as contact stress on the plate and the stress and displacement fields in the non-homogeneous medium are obtained for different materials.

Key words: Exponentially graded material, rigid plate, penny-shaped crack, transversely isotropic space, wave propagation

1. Introduction

Several experimental studies show that the analytical models are able to predict the stiffness and damping of the soil beneath a foundation with a reasonable degree of accuracy, e.g. [1-2]. Indeed, the experimental investigations are fundamental bases for proving the validation of a new procedure to consider the Soil-Structure Interaction (SSI) under dynamic loading for the design of structural elements such as machine foundation, transmitting tower foundation, and anchors. An exact formulation for the stiffness of the soil beneath a foundation can provide a practical tool for analyzing the soil-structure coupling by means of lumped parameters. In this approach, the effect of the soil-foundation interface is accounted for through a system of springs and dashpots assembled together with the superstructure stiffness [3-5]. Therefore, a complex analysis associated with continuum modeling of soil and soil-foundation interface may be reduced to a discrete analysis performed with a finite degree of freedoms.

Furthermore, from a mathematical perspective, taking an appropriate geometry as a domain of the problem is a crucial step to achieve the desired accuracy for an engineering problem. In foundation engineering, there are several examples in practice where the interaction of foundation with a full-space as a domain of the boundary value problem may lead to precise evaluation of lumped parameters resulted from SSI analysis. As an example, we mention the design of the foundation for an offshore wind turbine which is an application of SSI analysis based on substructure method [6-7]. In order to resist dynamic forces caused by the rotor, wind waves, or ocean waves, several types of deep foundations are employed depending on the water depth and the strength of the dynamic loading (e.g. embedded raft, mono-pile, mono-pile with guy wires, tripod, suction caisson, etc.). Among them, the foundation system consisting of a mono-pile supported by guy wires or tripod structures are common alternatives [8]; these are used for medium range water depths namely between 20m to 40m. This type of the foundation can mathematically be represented by a pile foundation embedded in the seabed and braced with several side anchors, see Fig. 1. Clearly, due to high depth of embedment, by analyzing the interaction of foundation with a full-space medium, one can correctly predict the behavior of side anchors.

Due to the sedimentation of the geological material, the structure of soil or rock generally possesses a certain degree of anisotropy and heterogeneous nature [9]; therefore, to estimate the dynamic stiffness of the embedded foundation, the constitutive model taking into account the non-uniformity and anisotropy of the material is required[10]. The complexity of the analysis related to the foundation-structure system will substantially increase if the contact conditions at the interface of the foundation and the soil are altered as a result of severe wave motion. The loss of perfect bonding between the soil and the foundation then significantly changes the dynamic properties of the foundation-structure system, an aspect typically disregarded in the design of foundations [11]. For instance, if the structural characteristics of the wind turbine, including the natural frequency and damping, are changed due to the detachment of the foundation, an unexpected and destructive vibration (resonance) may take

place [12]. Hence, a rigorous investigation of the dynamic impedance of the embedded foundation under various contact conditions could markedly eliminate the uncertainty existent in its design.

In view of the engineering applications mentioned above, and mathematical challenges, both elastostatic and elastodynamic boundary value problems of continua containing cracks and/or rigid plates have been of interest. Interestingly, the boundary value problems of an elastic material containing rigid circular thin plate and penny-shaped crack are mathematically the same. So far, the problem of a crack embedded in an inhomogeneous material was investigated by several authors for plane [13-15] or anti-plane [16-18] geometry. However, the case of three-dimensional analysis of continuum containing crack with a sharp gradient of shear properties of material at the vicinity of crack has been considered to a lesser degree [19]. The present paper is concerned with a more complicated problem due to existence of both rigid plate and penny-shaped cracks next to the plate in a continuously inhomogeneous transversely isotropic full-space; where, Due to the presence of the crack, the load bearing capacity of the rigid plate markedly decreases in comparison to the plate surrounded fully by the medium [20]. The three-dimensional elasticity problem of this paper was first investigated in [21] for axisymmetric movement of a penny-shaped inclusion (plate) located at the interface of two identical isotropic homogeneous half-space. The contact region of inclusion is supposed to be attached only to one half-space material and to be free from contact stress on the other face. Of course, the continuity of displacements and stresses is secured after the inclusion area. The method of integral transform was employed in [21] to reduce the problem to the evaluation of singular integral equations, whose solutions are obtained with the aid of Riemann-Hilbert problem. The assumption of the smooth contact condition between the inclusion and the upper half-space has been investigated in [22] and the corresponding results are similar to those of [21] for a wide range of Poisson's ratio. In the case of a plane problem, with the aid of complex potentials, a compact analytical solution was derived in [20]. This method was extended to account for the vertical movement of a rigid anchor placed at the interface of a bi-material full-plane in [24], which presented explicit results for all physical quantities of the problem. Later, three-dimensional mixed boundary value problems for bi-material full-space including both perfect and partial bounding of inclusion with the surrounding material have been examined in [25], where it was demonstrated that the oscillatory state of the contact stress at the edge of the inclusion could vanish when two half-spaces were filled with incompressible materials even though their shear moduli were different.

To the best the authors' knowledge, in the context of wave propagation induced by vibration of a rigid plate, the analytical solutions have not been fully developed for different boundary value problems in elastodynamics. This issue is further complicated if the materials experience a certain degree of anisotropy and spatial material gradient. Forced vertical and

rocking vibration of rigid circular foundation on a semi-infinite Gibson Soil have been formulated in [26-27]. Vertical vibration for a disc embedded at an arbitrary position in an isotropic half-space was examined in [28], and later, by means of potential functions, the problem has been generalized in [29] to a heterogeneous material with a quadratic variation of shear modulus in depth. The dynamic mechanical properties of a rigid circular disc and also a disc-shaped crack inside a transversely isotropic half-space have been studied in [30-32]. It was shown that the dynamic behavior of continuously inhomogeneous materials of infinite extent domains can be simulated by analyzing a number of limited layers and satisfying boundary conditions between them, with a finding that the number of layers should increase to ensure the accuracy of results in high-frequency oscillation [33].

The main goal of this paper is to examine the dynamic indentation of a rigid circular plate embedded in a non-homogeneous transversely isotropic full-space. The material's properties are increased exponentially through depths of each material. The governing equations of motion for the exponentially graded transversely isotropic material are decoupled with the aid of displacement potential functions recently introduced in [34]. This translates the equations of motion to a fourth order partial differential equation, whose solution is determined by Hankel integral transforms. Imposing traction and displacement boundary conditions on both sides of the plate and invoking the continuity of quantities outside the contact region simplifies the governing equations to a set of coupled singular integral equations. Due to the complexity of problems in dynamic cases, a numerical procedure is employed to solve singular integral equations. However, a reduced case of integral equations is prone to be analytically assessed. It is observed that the contact stress distributions around the edge of the plate possess highly oscillatory singularity, which is shown to be consistent with the results formerly obtained for isotropic materials.

2. Problem Definition

Full-space consists of two exponentially graded transversely isotropic material is taken as the domain of the boundary value problem involved in this paper. The plane of isotropy is assumed to be perpendicular to the vertical axis. A cylindrical coordinate system (r,θ,z) is set up in such a way that the *z*-axis is normal to the plane of isotropy, and the material properties c_{ij} and the mass density ρ are written in the form [34]

$$\rho(z)=\rho_0 e^{\beta_s z}, \qquad c_{ij}(z)=c_{0ij}e^{\beta_s z}, \; i=I,II, \tag{1}$$

where ρ_0 is the initiate value for the material density at $z=0$ and c_{0ij} (c_{011}, c_{012}, c_{013}, c_{033}, and c_{044}) are initial values for the elasticity constants. And $\tilde{\ }$ $\tilde{\ }$ with $\beta_s>0$ are non-homogeneity parameters where I and II denote the lower half-space (

$z>0$) and upper half-space ($z<0$) respectively. A rigid circular disc of the radius a and zero thickness is placed at the coordinate system's origin as a plate, while a penny-shaped crack, of the same radius as the plate, is faced to the side* $z=0^+$ of the rigid disc see Fig. 2. The plate undergoes a prescribed time-harmonic vertical vibration ω. The contact area above the plate is perfectly bonded to the upper material but weakened by a penny-shaped crack beneath the plate.

This gives a BVP with governing equations of motion for such medium in terms of displacements as following [34]

$$\begin{aligned} &c_{011}\left(\frac{\partial^2 u_r^i}{\partial r^2}+\frac{1}{r}\frac{\partial u_r^i}{\partial r}-\frac{u_r^i}{r^2}\right)+c_{044}\frac{\partial^2 u_r^i}{\partial z^2}+\left(c_{013}+c_{044}\right)\frac{\partial^2 u_z^i}{\partial r\partial z}+2\tilde{\mu}_i c\left(\frac{u_r^i}{\partial z}+\frac{\partial u_z^i}{\partial r}\right)=-\rho_0\omega^2 u_r^i \\ &c_{044}\left(\frac{\partial^2 u_z^i}{\partial r^2}+\frac{1}{r}\frac{\partial u_z^i}{\partial r}\right)+\left(c_{013}+c_{044}\right)\left(\frac{\partial^2 u_r^i}{\partial r\partial z}+\frac{1}{r}\frac{\partial u_r^i}{\partial z}\right)+c_{033}\frac{\partial^2 u_z^i}{\partial z^2}+2\tilde{\mu}_i c\left(\frac{u_r^i}{\partial r}+\frac{u_r^i}{r}\right) \qquad i=I,II \quad (2) \\ &\qquad\qquad +2\tilde{\mu}_i c\left(\frac{u_z^i}{\partial z}\right)=-\rho_0\omega^2 u_z^i \end{aligned}$$

in which u_r^i and u_z^i are the components of displacement vector in the cylindrical coordinate system for $i=I,II$ respectively, while ω is the circular frequency of motion. With boundary condition at $z=0$

$$u_r^{II}\left(r,0^-\right)=0, \qquad r<a \quad (3)$$

$$u_z^{II}\left(r,0^-\right)=\Delta e^{i\omega t}, \qquad r<a \quad (4)$$

$$\sigma_{zr}^{I}\left(r,0^+\right)=0, \qquad r<a \quad (5)$$

$$\sigma_{zz}^{I}\left(r,0^+\right)=0, \qquad r<a \quad (6)$$

$$u_i^{II}\left(r,0^-\right)=u_i^{I}\left(r,0^+\right), \qquad i=r,z \qquad r\geq a \quad (7)$$

* We define $0^+=\lim_{z\to 0^+} z$.

$$\sigma_{zi}^{II}\left(r,0^{-}\right)=\sigma_{zi}^{I}\left(r,0^{+}\right),\qquad i=r,z\qquad r\geq a, \tag{8}$$

and radiation conditions at infinity. Where Δ is the amplitudes of the displacement excitations, and $f(r,0^{\pm})=\lim_{z\to 0^{\pm}} f(r,z)$. It is worth mentioning that the numerical procedure implemented in this paper is carried out in non-dimensional form with no restriction for the magnitude of the variable Δ.

3. Method of Potential Functions

To solve the BVP, we use the displacement potential function $F^{i}(r,z,\omega), i=I,II$ introduced in [34], being applicable to irrotational axisymmetric dynamic boundary value problems of a transversely isotropic material as well as an isotropic material. This function is utilized to decouple the governing equation. In this way, the non-zero displacements u_r^i and u_z^i are expressed in terms of $F^{i}(r,z,\omega), i=I,II$ as [34]

$$\begin{aligned} u_r^i &= -\alpha_3 \frac{\partial^2 F^i}{\partial r \partial z} - 2\alpha_2 \tilde{\mu}_i \frac{\partial F^i}{\partial r} \\ u_z^i &= \left((1+\alpha_1)\nabla_{r\theta}^2 + \alpha_2 \frac{\partial}{\partial z}(2\tilde{\mu}_i \frac{\partial}{\partial z}) + \bar{\rho}_0 \omega^2 \right) F^i, \quad i=I,II \end{aligned} \tag{9}$$

where

$$\alpha_1 = \frac{c_{011}-c_{066}}{c_{066}}, \qquad \alpha_2 = \frac{c_{044}}{c_{066}}, \qquad \alpha_3 = \frac{c_{013}+c_{044}}{c_{066}}, \qquad \bar{\rho}_0 = \frac{\rho_0}{c_{066}}, \tag{10}$$

$$\nabla_{r\theta}^2 = \frac{\partial^2}{\partial r^2} + \frac{1}{r}\frac{\partial}{\partial r}. \tag{11}$$

In the above c_{066} is defined as $(c_{011}-c_{012})/2$. Substituting the displacements from (9) into the equations of motion (2) results in the following equation for the potential function $F^{i}(r,z,\omega), i=I,II$ [34]

$$\left[\square_i \square_i \quad {}^{2}\tilde{\lambda}_i \quad r \quad z \quad \tilde{}_i \right] F^i \quad i \quad I, II \tag{12}$$

where

$$\square \quad \left(\frac{\partial^2}{\partial z^2}\right)_\beta - \frac{\tilde{\lambda}}{s_j^2} + \frac{}{\mu_j}\omega^2, \ j = 1,2 \ , \ i = I, II \tag{13}$$

$$\left(\frac{\partial^n}{\partial z^n}\right)_{\tilde{}} \quad Y = e^{-\tilde{}} \frac{}{\partial z^n} (e^{\tilde{}} \ ), \tag{14}$$

$$\delta = \bar{\rho}_0 \left[-\frac{1}{\mu_1 s_2^2} \frac{1}{\mu_2 s_1^2} + \frac{1}{1+\alpha_1}\left(1+\frac{\alpha_4}{\alpha_2}\right)\right], \tag{15}$$

$$\mu_0 = 1, \qquad \mu_1 = \frac{c_{044}}{c_{066}}, \qquad \mu_2 = \frac{c_{011}}{c_{066}}.$$

in which s_1^2 and s_2^2 are the roots of

$$\alpha_4\alpha_2 s^4 + \left(\alpha_3^2 - \alpha_2^2 - (1+\alpha_1)\alpha_4\right)s^2 + \alpha_2(1+\alpha_1) = 0. \tag{16}$$

Similarly, the non-zero components of the stress tensor involved in imposing the axisymmetric boundary conditions are defined in terms of the potential function $F^i(r,z,\omega), i = I, II$ as follows [34]

$$\sigma_{zr}^i = \left(c_{044}\xi \left[-\alpha_2 \frac{d^2}{dz^2} - \bar{\rho}_0\omega^2 + \xi^2\left(1+\alpha_1\right) + \alpha_3 \frac{d^2}{dz^2}\right] F^i \right) e^{2\tilde{}_i z}, \ \ i = I, II \tag{17}$$

$$\sigma_{zz}^i = \left(c_{033} \frac{d}{dz}\left(\alpha_2 - \frac{d}{dz}(2\tilde{}_i \quad \frac{d}{dz} \right. \right. \quad c \quad ` F^i \quad \tilde{}_i c \quad F^i \quad ` e^{\ i z} \quad i \quad I \ II \tag{18}$$

Taking into account the nature of the problem, a zero-order Hankel integral transform with respect to the radial coordinate is applied to the equation (12), and the following ordinary differential equation is obtained for the transformed of the potential function $F^i(r,z,\omega), i = I, II$

$$\left[\square_i \square_i \quad \tilde{\lambda}_i \quad z \quad \tilde{\lambda}_i \right] F^i \qquad i = I, II \tag{19}$$

where

$$\square \quad \left(\frac{d^2}{dz^2} \right)_\beta - \frac{\tilde{\lambda}}{s_j^2} + \frac{}{\mu_j} \omega^2, \qquad j = 1,2, \quad i = I, II \tag{20}$$

and $F^{i0}(\xi, z, \omega), i = I, II$ is the zero-order Hankel integral transform of $F^i(r, z, \omega), \ i = I, II$. It results in the following general solutions for the equation (19)

$$F^{i0}(\xi, z, \omega) = e^{-\tilde{\lambda}_i z} \left[C_-^i(\xi) e^{-\lambda_1^i z} + D_-^i(\xi) e^{-\lambda_2^i z} + C_+^i(\xi) e^{\lambda_1^i z} + D_+^i(\xi) e^{\lambda_2^i z} \right], \ \ i = I, II \tag{21}$$

where

$$\lambda_j^i = \sqrt{a\xi^2 + b^i \pm \frac{1}{2}\sqrt{c\xi^4 + d^i \xi^2 + e}} \ , \ j = 1,2 \tag{22}$$

and

$$a = \frac{1}{2}\left(s_1^2 + s_2^2\right), \ b^i = \tilde{\lambda} \qquad \angle \left(\frac{1}{\alpha_4} + \frac{1}{\alpha_2} \right), \ c = (s_1^2 - s_2^2)^2$$

$$d^i = -16 \frac{\alpha_3 - \alpha_2}{\alpha_4} \tilde{\lambda} \qquad ^2 \left[\left(\frac{1}{\alpha_4} + \frac{1}{\alpha_2} \right)\left(s_1^2 + s_2^2\right) - 2\frac{1+\alpha_1}{\alpha_4}\left(\frac{1}{1+\alpha_1} + \frac{1}{\alpha_2} \right) \right], \quad i = I, II \tag{23}$$

$$e = \bar{\rho}_0^2 \omega^4 \left(\frac{1}{\alpha_4} - \frac{1}{\alpha_2} \right)^2 .$$

And $C_-^i(\xi), D_-^i(\xi), C_+^i(\xi)$ and $D_+^i(\xi)$ are unknown coefficients determined from boundary conditions. As seen from (22), λ_1^i and λ_2^i are radical functions, and hence are multi-valued functions. To be consistent with (21), one must define a Riemann surface with two sheets such that λ_1 and λ_2 are single-valued and analytically continuous from one sheet to another. This can be achieved by specifying the branch cuts for λ_1^i and λ_2^i on the complex ξ-plane, with the branch points emanating from zeros of these functions, or from the equation of $\lambda_1^i = \lambda_2^i$ (e.g., see [33]). Under these choices of the branches and taking into account the radiation condition, the $e^{(\lambda_1^I - \tilde{\lambda}_I) z}$ and $e^{(\lambda_2^i - \tilde{\lambda}_i) z}$ terms become inadmissible and consequently

$C_+^I(\xi)$ and $D_+^I(\xi)$ in Eq. (21) vanish. It is worthwhile mentioning that through a similar analysis for the upper half space, $C_-^{II}(\xi)$ and $D_-^{II}(\xi)$ are vanished. In the sequel, for convenient, we name unknown coefficients of each medium as $A_1(\xi)=C_-^I(\xi), B_1(\xi)=D_-^I(\xi)$ and $A_2(\xi)=C_+^{II}(\xi), B_2(\xi)=D_+^{II}(\xi)$.

Now, with the aid of appropriate inverse Hankel integral transforms and rearranging the equations (9) and (17-18), the solutions for the stress and displacement fields throughout the full-space region are obtained in explicit forms as

$$u_r^I(r,z)=\int_0^\infty (A_1(\xi)\varphi_{12}^I e^{-(\lambda_1^I+\tilde{\jmath}_I)z}+B_1(\xi)\psi_{22}^I e^{(\lambda_1^I-\tilde{\jmath}_I)z})\xi J_1(r\xi)d\xi \tag{24}$$

$$u_z^I(r,z)=\int_0^\infty (A_1(\xi)\vartheta_1^I e^{-(\lambda_1^I+\tilde{\jmath}_I)z}+B_1(\xi)\upsilon_2^I e^{(\lambda_1^I-\tilde{\jmath}_I)z})\xi J_0(r\xi)d\xi \tag{25}$$

$$\sigma_{zr}^I(r,z)=\int_0^\infty (A_1(\xi)c_{066}(z)\eta_{12}^I\xi e^{-(\lambda_1^I+\tilde{\jmath}_I)z}+B_1(\xi)c_{066}(z)\mu_{22}^I\xi e^{(\lambda_1^I-\tilde{\jmath}_I)z})\xi J_1(r\xi)d\xi \tag{26}$$

$$\sigma_{zz}^I(r,z)=\int_0^\infty (A_1(\xi)c_{066}(z)\nu_{12}^I e^{-(\lambda_1^I+\tilde{\jmath}_I)z}+B_1(\xi)c_{066}(z)\nu_{22}^I e^{(\lambda_1^I-\tilde{\jmath}_I)z})\xi J_0(r\xi)d\xi \tag{27}$$

for the lower half-space called Region I, and

$$u_r^{II}(r,z)=\int_0^\infty (A_2(\xi)\varphi_{11}^{II} e^{(\lambda_1^{II}-\tilde{\jmath}_{II})z}+B_2(\xi)\psi_{21}^{II} e^{-(\lambda_1^{II}-\tilde{\jmath}_{II})z})\xi J_1(r\xi)d\xi \tag{28}$$

$$u_z^{II}(r,z)=\int_0^\infty (A_2(\xi)\vartheta_1^{II} e^{(\lambda_1^{II}-\tilde{\jmath}_{II})z}+B_2(\xi)\upsilon_2^{II} e^{-(\lambda_1^{II}-\tilde{\jmath}_{II})z})\xi J_0(r\xi)d\xi \tag{29}$$

$$\sigma_{zr}^{II}(r,z)=\int_0^\infty (A_2(\xi)c_{066}(z)\eta_{11}^{II} e^{(\lambda_1^{II}-\tilde{\jmath}_{II})z}+B_2(\xi)c_{066}(z)\mu_{21}^{II} e^{-(\lambda_1^{II}-\tilde{\jmath}_{II})z})\xi J_1(r\xi)d\xi \tag{30}$$

$$\sigma_{zz}^{II}(r,z)=\int_0^\infty (A_2(\xi)c_{066}(z)\nu_{11}^{II} e^{(\lambda_1^{II}-\tilde{\jmath}_{II})z}+B_2(\xi)c_{066}(z)\nu_{21}^{II} e^{-(\lambda_1^{II}-\tilde{\jmath}_{II})z})\xi J_0(r\xi)d\xi \tag{31}$$

for the upper half-space called Region II. In the relations (24) to (31), we have $c_{066}(z)=(c_{011}(z)-c_{012}(z))/2$, $A_j(\xi)$ and $B_j(\xi)$ j=1,2 are unknown Hankel parameters corresponding to the lower and upper half-space, and following relations:

$$
\begin{aligned}
&\lambda_j^I=\lambda_j^{II}=\lambda_j;\vartheta_j^I=\vartheta_j^{II}=\vartheta_j\\
&\varphi_{j1}^I=-\varphi_{j2}^{II}=\varphi_{j1};\varphi_{j2}^I=-\varphi_{j1}^{II}=\varphi_{j2}\\
&\eta_{j1}^I=\eta_{j2}^{II}=\eta_{j1};\eta_{j2}^I=\eta_{j1}^{II}=\eta_{j2}\\
&\nu_{j1}^I=-\nu_{j2}^{II}=\nu_{j1};\nu_{j2}^I=-\nu_{j1}^{II}=\nu_{j2}\\
&\vartheta_j=\alpha_2\left(\lambda_j^2-\beta_s^2\right)+\rho_0\omega^2-\xi^2(1+\alpha_1)\\
&\varphi_{j1}=2\alpha_2\beta_s+\alpha_3(\lambda_j-\beta_s)\\
&\varphi_{j2}=2\alpha_2\beta_s-\alpha_3(\lambda_j+\beta_s)\\
&\eta_{j1}=\alpha_2(\alpha_3(\lambda_j-\beta_s)^2+2\alpha_2\beta_s(\lambda_j-\beta_s)-\vartheta_j)\\
&\eta_{j2}=\alpha_2(\alpha_3(\lambda_j+\beta_s)^2-2\alpha_2\beta_s(\lambda_j+\beta_s)-\vartheta_j)\\
&\nu_{j1}=(\alpha_3\left(\alpha_3-\alpha_2\right)\xi^2+\alpha_4\vartheta_j)(\lambda_j-\beta_s)+2\alpha_2\left(\alpha_3-\alpha_2\right)\beta_s\xi^2\\
&\nu_{j2}=-(\alpha_3\left(\alpha_3-\alpha_2\right)\xi^2+\alpha_4\vartheta_j)(\lambda_j+\beta_s)+2\alpha_2\left(\alpha_3-\alpha_2\right)\beta_s\xi^2\\
&j=1,2.
\end{aligned}
\tag{32}
$$

In the above, we have used $\tilde{\ }$ $\tilde{\ }$ to simplify the relations.

4. Formulating of mixed boundary value problem

After obtaining displacements and stresses fields in terms of potential functions, imposing radiation condition, one can obtain unknown coefficients $A_j(\xi)$ and $B_j(\xi)$ j=1,2 by imposing the mixed boundary conditions at the interface of two half-space. In the domain inside the plate and at the interface of two joined half-space, the mixed boundary value problem in conjunction with the equations (3) to (6) and (26) to (29) reads as

$$u_r^{II}(r,0^-)=\int_0^\infty(\varphi_{11}^{II}\xi^2A_2(\xi)+\varphi_{21}^{II}\xi^2B_2(\xi))J_1(r\xi)d\xi=0, \tag{33}$$

$$u_z^{II}(r,0^-)=\int_0^\infty(\vartheta_1^{II}\xi A_2(\xi)+\vartheta_2^{II}\xi B_2(\xi))J_0(r\xi)d\xi=\Delta, \tag{34}$$

$$\sigma_{zr}^{I}(r,0^{+})=\int_{0}^{\infty}\xi(c_{066}^{I}\eta_{12}^{I}\xi A_{1}(\xi)+c_{066}^{I}\eta_{22}^{I}\xi B_{1}(\xi))J_{1}(r\xi)d\xi=0, \tag{35}$$

$$\sigma_{zz}^{I}(r,0^{+})=\int_{0}^{\infty}\xi(c_{066}^{I}\nu_{12}^{I}A_{1}(\xi)+c_{066}^{I}\nu_{22}^{I}B_{1}(\xi))J_{0}(r\xi)d\xi=0. \tag{36}$$

Where Δ is the amplitude of vibration, which also appeared in the equation (4). In addition, the continuity of the stress and displacement fields exterior to the plate area implies that

$$\Delta u_{r}(r,0)=\int_{0}^{\infty}(\varphi_{12}^{I}\xi^{2}A_{1}(\xi)+\varphi_{22}^{I}\xi^{2}B_{1}(\xi)-\varphi_{11}^{II}\xi^{2}A_{2}(\xi)-\varphi_{21}^{II}\xi^{2}B_{2}(\xi))J_{1}(r\xi)d\xi=0, \tag{37}$$

$$\Delta u_{z}(r,0)=\int_{0}^{\infty}(\vartheta_{1}^{I}\xi A_{1}(\xi)+\vartheta_{2}^{I}\xi B_{1}(\xi)-\vartheta_{1}^{II}\xi A_{2}(\xi)-\vartheta_{2}^{II}\xi B_{2}(\xi))J_{0}(r\xi)d\xi=0, \tag{38}$$

$$\Delta\sigma_{zr}(r,0)=\int_{0}^{\infty}\xi(c_{066}^{I}\eta_{12}^{I}\xi A_{1}(\xi)+c_{066}^{I}\eta_{22}^{I}\xi B_{1}(\xi)-c_{066}^{II}\eta_{11}^{II}\xi A_{2}(\xi)-c_{066}^{II}\eta_{21}^{II}\xi B_{2}(\xi))J_{1}(r\xi)d\xi=0, \tag{39}$$

$$\Delta\sigma_{zz}(r,0)=\int_{0}^{\infty}\xi(c_{066}^{I}\nu_{12}^{I}A_{1}(\xi)+c_{066}^{I}\nu_{22}^{I}B_{1}(\xi)-c_{066}^{II}\nu_{11}^{II}A_{2}(\xi)-c_{066}^{II}\nu_{21}^{II}B_{2}(\xi))J_{0}(r\xi)d\xi=0. \tag{40}$$

where $\Delta f(r,0)=f(r,0^{+})-f(r,0^{-})$. To further reduce the system of coupled mixed boundary conditions (33) to (40), one may benefit from introducing the following substitutions in equation (37) to (40)

$$S(\xi)=\varphi_{12}^{I}\xi^{2}A_{1}(\xi)+\varphi_{22}^{I}\xi^{2}B_{1}(\xi)-\varphi_{11}^{II}\xi^{2}A_{2}(\xi)-\varphi_{21}^{II}\xi^{2}B_{2}(\xi), \tag{41}$$

$$R(\xi)=\vartheta_{1}^{I}\xi A_{1}(\xi)+\vartheta_{2}^{I}\xi B_{1}(\xi)-\vartheta_{1}^{II}\xi A_{2}(\xi)-\vartheta_{2}^{II}\xi B_{2}(\xi), \tag{42}$$

$$Q(\xi)=c_{066}^{I}\eta_{12}^{I}\xi A_{1}(\xi)+c_{066}^{I}\eta_{22}^{I}\xi B_{1}(\xi)-c_{066}^{II}\eta_{11}^{II}\xi A_{2}(\xi)-c_{066}^{II}\eta_{21}^{II}\xi B_{2}(\xi), \tag{43}$$

$$P(\xi)=c_{066}^{I}\nu_{12}^{I}A_{1}(\xi)+c_{066}^{I}\nu_{22}^{I}B_{1}(\xi)-c_{066}^{II}\nu_{11}^{II}A_{2}(\xi)-c_{066}^{II}\nu_{21}^{II}B_{2}(\xi). \tag{44}$$

Now, following the elegant transformations introduced in [21], we write these functions in the following forms

$$P(\xi)=\int_0^a A(s)\cos(s\xi)ds,\quad Q(\xi)=\int_0^a B(s)\sin(s\xi)ds,$$
$$R(\xi)=\int_0^a \beta(s)\sin(s\xi)ds,\quad S(\xi)=\int_0^a \alpha(s)\cos(s\xi)ds. \tag{45}$$

Substituting the above relations into Eqs. (37) to (40) and using the certain identities presented in Appendix A, one may find that the equations (38) to (40) are automatically satisfied and the only restriction that is needed for satisfying equation (37) is as follow:

$$\int_0^a \alpha(s)ds=0. \tag{46}$$

It is noteworthy that the auxiliary functions $\alpha(s)$, $\beta(s)$, $A(s)$ and $B(s)$ could be extended to the negative domain in such a way that the functions $A(s)$ and $\alpha(s)$ have even properties and $B(s)$ and $\beta(s)$ possess odd properties. Writing $A_1(\xi)$, $A_2(\xi)$, $B_1(\xi)$ and $B_2(\xi)$ from (41) to (44) in terms of $P(\xi)$, $Q,(\xi)$ $R(\xi)$ and $S(\xi)$, using (32), and substituting the results into equations (33) to (36) leads to

$$u_r^{II}(r,0^-)=\int_0^\infty [a_{11}(\xi)S(\xi)+a_{12}(\xi)R(\xi)+a_{13}(\xi)Q(\xi)+a_{14}(\xi)P(\xi)]J_1(r\xi)d\xi=0, \tag{47}$$

$$u_z^{II}(r,0^-)=\int_0^\infty [a_{21}(\xi)S(\xi)+a_{22}(\xi)R(\xi)+a_{23}(\xi)Q(\xi)+a_{24}(\xi)P(\xi)]J_0(r\xi)d\xi=\Delta, \tag{48}$$

$$\sigma_{zr}^{I}(r,0^+)=\int_0^\infty \xi[a_{31}(\xi)S(\xi)+a_{32}(\xi)R(\xi)+a_{33}(\xi)Q(\xi)+a_{34}(\xi)P(\xi)]J_1(r\xi)d\xi=0, \tag{49}$$

$$\sigma_{zz}^{I}(r,0^+)=\int_0^\infty \xi[a_{41}(\xi)S(\xi)+a_{42}(\xi)R(\xi)+a_{43}(\xi)Q(\xi)+a_{44}(\xi)P(\xi)]J_0(r\xi)d\xi=0, \tag{50}$$

where the functions $a_{ij}(\xi)$ are as follows

$$a_{11}(\xi)=a_{22}(\xi)=-\frac{1}{2},\qquad a_{33}(\xi)=a_{44}(\xi)=\frac{1}{2}, \tag{51a}$$

$$a_{14}(\xi)=a_{23}(\xi)=a_{32}(\xi)=a_{41}(\xi)=0, \tag{51b}$$

$$a_{12}(\xi)=\frac{\xi(\eta_{22}\varphi_{12}-\eta_{12}\varphi_{22})}{2(\eta_{22}\vartheta_1-\eta_{12}\vartheta_2)},\quad a_{13}(\xi)=\frac{\xi(\vartheta_1\varphi_{22}-\vartheta_2\varphi_{12})}{2c_{066}(\eta_{22}\vartheta_1-\eta_{12}\vartheta_2)}, \tag{51c}$$

$$a_{21}(\xi)=\frac{\vartheta_1\upsilon_{22}-\vartheta_2\upsilon_{12}}{2\xi(\upsilon_{22}\varphi_{12}-\upsilon_{12}\varphi_{22})},\quad a_{24}(\xi)=\frac{\xi(\vartheta_2\varphi_{12}-\vartheta_1\varphi_{22})}{2c_{066}(\upsilon_{22}\varphi_{12}-\upsilon_{12}\varphi_{22})}, \tag{51d}$$

$$a_{31}(\xi)=\frac{c_{066}(\eta_{12}\upsilon_{22}-\eta_{22}\upsilon_{12})}{2\xi(\upsilon_{22}\varphi_{12}-\upsilon_{12}\varphi_{22})},\quad a_{34}(\xi)=\frac{\xi(\eta_{22}\varphi_{12}-\eta_{12}\varphi_{22})}{2(\upsilon_{22}\varphi_{12}-\upsilon_{12}\varphi_{22})}, \tag{51e}$$

$$a_{42}(\xi)=\frac{c_{066}(\eta_{22}\upsilon_{12}-\eta_{12}\upsilon_{22})}{2\xi(\eta_{22}\vartheta_1-\eta_{12}\vartheta_2)},\quad a_{43}(\xi)=\frac{\vartheta_1\upsilon_{22}-\vartheta_2\upsilon_{12}}{2\xi(\eta_{22}\vartheta_1-\eta_{12}\vartheta_2)}. \tag{51f}$$

It is convenient here to introduce the following four integral operators to express the result of equations (47) to (50) in the form of ordinary functions. Thus, define [21]

$$\begin{aligned} f_1(s;f(r))&=\frac{d}{ds}\int_0^s\frac{s f(r)\,\mathrm{d}r}{\sqrt{s^2-r^2}}, & f_2(s;f(r))&=\frac{d}{ds}\int_0^s\frac{r f(r)\,\mathrm{d}r}{\sqrt{s^2-r^2}},\\ f_3(s;f(r))&=\int_0^s\frac{s f(r)\,\mathrm{d}r}{\sqrt{s^2-r^2}}, & f_4(s;f(r))&=\int_0^s\frac{r f(r)\,\mathrm{d}r}{\sqrt{s^2-r^2}}. \end{aligned} \tag{52}$$

Applying these four operators on both sides of four equations (47) to (50), respectively, substituting the relationships given in equation (45), and using the odd and even properties of the integrals defined in (45), one may simplify the mixed boundary conditions (47) to (50) in the form of the following coupled singular integral equations

$$\frac{-L_{11}}{\pi}\int_{-a}^{a}\frac{\alpha(t)}{t-s}+L_{12}B(s)+L_{13}B(s)+\int_{-a}^{a}\left[k_{12}(t,s)\beta(t)+k_{13}(t,s)B(t)\right]dt=0, \tag{53}$$

$$L_{21}\alpha(s)+\frac{L_{22}}{\pi}\int_{-a}^{a}\frac{\beta(t)}{t-s}+L_{24}A(s)+\int_{-a}^{a}\left[k_{21}(t,s)\alpha(t)+k_{24}(t,s)A(t)\right]dt=\frac{2}{\pi}\Delta, \tag{54}$$

$$L_{31}\alpha(s)+\frac{L_{33}}{\pi}\int_{-a}^{a}\frac{B(t)}{t-s}+L_{34}A(s)+\int_{-a}^{a}\left[k_{31}(t,s)\alpha(t)+k_{34}(t,s)A(t)\right]dt=-\frac{2}{\pi}C, \tag{55}$$

$$L_{42}\beta(s)+L_{43}B(s)-\frac{L_{44}}{\pi}\int_{-a}^{a}\frac{A(t)}{t-s}+\int_{-a}^{a}\left[k_{42}(t,s)\beta(t)+k_{43}(t,s)B(t)\right]dt=0. \tag{56}$$

where the coefficients L_{ij} are defined as

$$L_{ij}=\lim_{\xi\to\infty}a_{ij}(\xi) \tag{57}$$

In addition, the kernel functions of integral equations are determined as

$$k_{12}(t,s)=\frac{L_{12}}{\pi}\int_0^{\infty}\left(\frac{a_{12}(\xi)}{L_{12}}-1\right)\sin(t\xi)\sin(s\xi)d\xi, \tag{58a}$$

$$k_{13}(t,s)=\frac{L_{13}}{\pi}\int_0^{\infty}\left(\frac{a_{13}(\xi)}{L_{13}}-1\right)\sin(t\xi)\sin(s\xi)d\xi, \tag{58b}$$

$$k_{21}(t,s)=\frac{L_{21}}{\pi}\int_0^{\infty}\left(\frac{a_{21}(\xi)}{L_{21}}-1\right)\cos(t\xi)\cos(s\xi)d\xi, \tag{58c}$$

$$k_{24}(t,s)=\frac{L_{24}}{\pi}\int_0^{\infty}\left(\frac{a_{24}(\xi)}{L_{24}}-1\right)\cos(t\xi)\cos(s\xi)d\xi, \tag{58d}$$

$$k_{31}(t,s)=\frac{L_{31}}{\pi}\int_0^{\infty}\left(\frac{a_{31}(\xi)}{L_{31}}-1\right)\cos(t\xi)\cos(s\xi)d\xi, \tag{58e}$$

$$k_{34}(t,s)=\frac{L_{34}}{\pi}\int_0^{\infty}\left(\frac{a_{34}(\xi)}{L_{24}}-1\right)\cos(t\xi)\cos(s\xi)d\xi, \tag{58f}$$

$$k_{42}(t,s)=\frac{L_{42}}{\pi}\int_0^{\infty}\left(\frac{a_{42}(\xi)}{L_{42}}-1\right)\sin(t\xi)\sin(s\xi)d\xi, \tag{58g}$$

$$k_{43}(t,s)=\frac{L_{43}}{\pi}\int_0^{\infty}\left(\frac{a_{43}(\xi)}{L_{43}}-1\right)\sin(t\xi)\sin(s\xi)d\xi. \tag{58h}$$

Constant C in the equation (55) appears after the integral operator $f_3(s;\ f(r))$ is applied on both sides of the equation (49). It is worthwhile to be mentioned that, in the analytical part, C can be obtained directly by satisfying equation (46). However, a computational procedure is required for obtaining constant C in general case(FGM under the static movement of the inclusion or dynamic case), which can be found in Appendix B.

The singular integral equations (53) to (56) consist of two parts, arising from the physical nature of the associated problem. The left-hand side of these equations contributes in forming of a homogeneous static solution of the problem while the remaining equations create a dynamic non-homogeneous contribution of mixed boundary conditions (see [34]).

From the solution of auxiliary functions, it is possible to derive an explicit relationship for contact stress on the top of the inclusion. By rewriting equations (39) and (40) for $0 \le r < a$, which define the contact traction between the inclusion and the medium, and implementing infinite integration, one may obtain

$$\Delta\sigma_{zr}(r,0) = \frac{d}{dr}\int_r^a \frac{B(s)ds}{\sqrt{s^2-r^2}}, \tag{59}$$

$$\Delta\sigma_{zz}(r,0) = \frac{1}{r}\frac{d}{dr}\int_r^a \frac{sA(s)ds}{\sqrt{s^2-r^2}}. \tag{60}$$

The total load needed to support the prescribed vertical displacement is usually of interest. This quantity has been determined by integrating the normal traction at the interface of the plate and the medium. Thus, the total load is expressed in terms of the solution for the auxiliary function $A(s)$ as

$$F = \int_0^{2\pi}\int_0^a \Delta\sigma_{zz}(r,0)\, r\, dr\, d\theta = -2\pi\int_0^a A(s)ds\,. \tag{61}$$

The singular integral equations (53)-(56) contain some complex kernels, which prevent determining an analytical solution. However, there are certain special cases for which closed-form solutions are possible.

5. Analytical solution for homogeneous transversally isotropic full-space

The singular integral equations obtained in the previous section will now be analytically solved for a special case of static movement of the plate located in a homogeneous transversely isotropic full-space. The closed-form solution could be pursued from the knowledge of the fact that the right-hand side of equations (53) to (56) vanishes if both the frequency of vibration and the non-homogeneity of material, characterized by the parameter β_s, tend to zero. In this case, it is required to introduce a modification factor inside the procedure outlined in the previous section. This is accomplished by multiplying both sides of equations (33) and (36) by the parameters $\sqrt{m}$ $(m > 0)$ and dividing both sides of equations (37) and (40) by the same value and keep other procedures unchanged. This results in certain useful relationships

$$L_{21}/L_{12}=m,\quad L_{22}/L_{11}=m,\quad L_{23}/L_{14}=m,\quad L_{24}/L_{13}=m,$$
$$L_{31}/L_{42}=m,\quad L_{32}/L_{14}=m,\quad L_{33}/L_{44}=m,\quad L_{34}/L_{43}=m. \tag{62}$$

We are now able to present a compact representation of equations (53) to (56) by multiplying the equations (53) and (56) to the complex parameters $m\times i$ (with $i=\sqrt{-1}$) and adding them to equations (54) and (55) to have

$$L_{21}\phi_2(s)+\frac{L_{22}}{\pi i}\int_{-a}^{a}\frac{\phi_2(t)}{t-s}dt+L_{24}\phi_1(s)=\frac{2}{\pi}\Delta, \tag{63}$$

$$L_{31}\phi_2(s)+\frac{L_{33}}{\pi i}\int_{-a}^{a}\frac{\phi_1(t)}{t-s}dt+L_{34}\phi_1(s)=-\frac{2}{\pi}C, \tag{64}$$

where

$$\phi_1(s)=A(s)+B(s)i,$$
$$\phi_2(s)=\alpha(t)+\beta(t)i. \tag{65}$$

Evidently, the equations (63) and (64) still contain coupling characteristics. To uncouple them, it is useful to multiply the equation (63) by an unknown parameter $\bar{\lambda}$ and add to the equation (64), which reads

$$(L_{34}-\bar{\lambda}L_{24})\phi_1(s)+(L_{31}-\bar{\lambda}L_{21})\phi_2(s)+\frac{1}{\pi i}\int_{-a}^{a}\frac{L_{33}\phi_1(t)-\bar{\lambda}L_{22}\phi_2(t)}{t-s}dt=-\frac{2}{\pi}(\bar{\lambda}\Delta+C). \tag{66}$$

The equation (66) may be written in two separate classical singular integral equations if the following relationship is confirmed [25]

$$\frac{(L_{31}-\bar{\lambda}L_{21})}{(L_{34}-\bar{\lambda}L_{24})}=\frac{-\bar{\lambda}L_{22}}{L_{33}}. \tag{67}$$

This is a quadratic equation, yielding two roots for the parameter $\bar{\lambda}$, which after some algebraic manipulations and benefitting from the relation $L_{22}=-L_{33}=-1/2$ result in

$$\bar{\lambda}_1=i\sqrt{\frac{L_{31}}{L_{24}}},\quad \bar{\lambda}_2=-i\sqrt{\frac{L_{31}}{L_{24}}}. \tag{68}$$

Effective representations are thus defined as

$$X_j(s) = \phi_1(s) + \bar{\lambda}_j \phi_2(s), \qquad j=1,2, \tag{69}$$

which helps to simplify the equation (70) to

$$X_j(s) + \frac{\gamma_j}{\pi i} \int_{-a}^{a} \frac{X_j(t)}{t-s} dt = e_j, \qquad j=1,2, \tag{70}$$

where

$$\gamma_j = \frac{1}{2(L_{34} - \bar{\lambda}_j L_{24})}, \quad e_j = \frac{-2}{\pi} \frac{(\bar{\lambda}_j \Delta + C)}{(L_{34} - \bar{\lambda}_j L_{24})}. \tag{71}$$

The procedure for obtaining a closed-form solution for equation (70) is based on the Riemann-Hilbert problem in the complex plane (see [25]). Avoiding the details (see [21] and [25]), the analytical solution emerges as

$$X_j(s) = \frac{e_j}{(1+\gamma_j) e^{\pi \bar{\alpha}_j}} \left(\frac{a-s}{a+s}\right)^{i\bar{\alpha}_j}, \qquad j=1,2, \tag{72}$$

where

$$\bar{\alpha}_j = \left(\frac{1}{2\pi}\right) Ln\left(\frac{1-\gamma_j}{1+\gamma_j}\right), \qquad j=1,2. \tag{73}$$

The mandatory constraint on the integral equation, equation (46), based on the new representation is formed in the following form

$$\int_{-a}^{a} \frac{X_2(s) - X_1(s)}{\bar{\lambda}_2 - \bar{\lambda}_1} ds = 0. \tag{74}$$

With the knowledge of the analytical solution, the unknown coefficient of integration C is specified analytically as

$$C = \left(\frac{K\bar{\lambda}_2 - \bar{\lambda}_1}{1-K}\right)\Delta, \tag{75}$$

where

$$K = \frac{(1+\gamma_1)\overline{\alpha_2}\,sinh\,(\pi\overline{\alpha_1})e^{\pi\overline{\alpha_1}}}{(1+\gamma_2)\overline{\alpha_1}\,sinh\,(\pi\overline{\alpha_2})e^{\pi\overline{\alpha_2}}}. \tag{76}$$

Similarly, the total load [see Eqn. (61)] is expressed in the new representation as

$$F = -\pi\int_{-a}^{a}\frac{(\overline{\lambda}_2 X_1(s) - \overline{\lambda}_1 X_2(s))}{(\overline{\lambda}_2 - \overline{\lambda}_1)}ds\,. \tag{77}$$

This results in

$$F = \frac{-2\pi^2 a}{(\overline{\lambda}_2 - \overline{\lambda}_1)}\left(\frac{\overline{\lambda}_2\overline{\alpha}_1 e_1}{(1+\gamma_1)sinh\,(\pi\overline{\alpha_1})e^{\pi\overline{\alpha_1}}} - \frac{\overline{\lambda}_1\overline{\alpha}_2 e_2}{(1+\gamma_2)sinh\,(\pi\overline{\alpha_2})e^{\pi\overline{\alpha_2}}}\right). \tag{78}$$

In order to determine analytical solutions for other physical variables, including displacement and stress functions inside the homogeneous transversely isotropic material, it is required to obtain a closed-form expression for the unknown functions presented in equation (45). By substituting the solutions of auxiliary functions, equation (72), and their other representation in equation (65), inside the right-hand side of equation (72) and taking the advantage of the identity presented in Appendix A [36], a closed-form solution for the unknown functions of the problem is found. Employing this identity eventually leads to the explicit solution of unknown functions in equation (45) as

$$\begin{aligned} P(\xi) = \mathrm{Re}\{&\frac{\overline{\lambda}_2 e_1}{4(1+\gamma_1)(\overline{\lambda}_2 - \overline{\lambda}_1)e^{\pi\overline{\alpha_1}}}[H(a,\overline{\alpha}_1,\xi) + H(a,\overline{\alpha}_1,-\xi)] \\ &\frac{\overline{\lambda}_1 e_2}{4(1+\gamma_2)(\overline{\lambda}_2 - \overline{\lambda}_1)e^{\pi\overline{\alpha_2}}}[H(a,\overline{\alpha}_2,\xi) + H(a,\overline{\alpha}_2,-\xi)]\}, \end{aligned} \tag{79}$$

$$\begin{aligned} Q(\xi) = \mathrm{Im}\{&\frac{\overline{\lambda}_2 e_1}{4i(1+\gamma_1)(\overline{\lambda}_2 - \overline{\lambda}_1)e^{\pi\overline{\alpha_1}}}[H(a,\overline{\alpha}_1,-\xi) - H(a,\overline{\alpha}_1,\xi)] \\ &\frac{\overline{\lambda}_1 e_2}{4i(1+\gamma_2)(\overline{\lambda}_2 - \overline{\lambda}_1)e^{\pi\overline{\alpha_2}}}[H(a,\overline{\alpha}_2,-\xi) - H(a,\overline{\alpha}_2,\xi)]\}, \end{aligned} \tag{80}$$

$$R(\xi)=\mathrm{Im}\{\frac{-e_1}{4i(1+\gamma_1)(\overline{\lambda}_2-\overline{\lambda}_1)e^{\pi\overline{\alpha}_1}}[H(a,\overline{\alpha}_1,-\xi)-H(a,\overline{\alpha}_1,\xi)] + \frac{e_2}{4i(1+\gamma_2)(\overline{\lambda}_2-\overline{\lambda}_1)e^{\pi\overline{\alpha}_2}}[H(a,\overline{\alpha}_1,-\xi)-H(a,\overline{\alpha}_1,\xi)]\}, \tag{81}$$

$$S(\xi)=\mathrm{Re}\{\frac{-e_1}{4(1+\gamma_1)(\overline{\lambda}_2-\overline{\lambda}_1)e^{\pi\overline{\alpha}_1}}[H(a,\overline{\alpha}_1,\xi)+H(a,\overline{\alpha}_1,-\xi)]. \tag{82}$$

It is now possible to find the displacement and stress functions by substituting equations (79)-(82) in equations (41)-(44) and implementing the infinite integrals embedded in the Hankel transform of equations (24)-(31). Due to the complexity of confluent hypergeometric function, the use of numerical integration for estimation of field's variables is inevitable.

In the special case of an isotropic material, the elasticity coefficients of transversely isotropic material are written as

$$c_{11}=c_{13}=\frac{E(1-\nu)}{(1+\nu)(1-2\nu)},\quad c_{12}=c_{33}=\frac{E\nu}{(1+\nu)(1-2\nu)},\quad c_{44}=c_{66}=\frac{E}{2(1+\nu)}=G, \tag{83}$$
$$s_0=s_1=s_2=1,$$

with E and G being the Young and shear moduli and ν the Poisson ratio. This leads to the compact solution for the unknown coefficient of integration and total vertical load on the plate. Simplifying the associated relationships yields

$$C=\frac{Ln(3-4\nu)\Delta}{\pi\sqrt{3-4\nu}}, \tag{84}$$

$$F=4G\pi a\Delta\frac{1+[\frac{Ln(3-4\nu)}{\pi}]^2}{\sqrt{3-4\nu}}. \tag{85}$$

This is in agreement with the analytical solution presented in [21] for the vertical movement of a thin rigid inclusion partially surrounded by penny-shaped crack and inside isotropic full-space. It is noteworthy to mention that, in Keer's solution, the imposed vertical displacement is assumed to be divided by twice of shear modulus G .

6. Computational results

This section is devoted to a numerical treatment of singular integral equation in the general case. The numerical calculation of the integral equation seems to be inevitable since the right-hand side of the equations (53)-(56) possesses dynamic non-homogeneous kernels of an infinite integral. Generally, there will be two branch points lying on the formal path of integration of the integrals (58) which needs to be located and considered during the integration procedure. Due to the existence of the Cauchy singularity in the kernel of an integral equation, the conventional quadrature method cannot yield a reliable solution [38]. In this paper, we numerically estimate the solution of integral equations by means of expanding unknown functions in terms of appropriate functions. The analytical static solution for the problem reveals that the result of auxiliary functions tends to have a singular point around the edge of the plate at $r = a$. To take into account such singularity in dynamic non-homogeneous case, we utilize Chebyshev polynomials as expanding functions so that the singularity at the edge of the plate is approximated accurately. By selecting a set of appropriate collocation points, some linear equations will be provided, which eventually result in the unknown coefficients of expansions. The details of the collocation method involved are presented in the Appendix B. To be able to demonstrate the effectiveness of the aforementioned procedure, a number of exponentially graded transversely isotropic materials have been introduced in Table 1 and corresponding numerical results will next be presented.

In Table 1 the parameters E, E', G, G', ν and ν' are the engineering constants of materials and have direct relations with the elasticity constants of transversely isotropic medium as

$$
\begin{aligned}
c_{011} &= \frac{E\left(1-E\nu'^2/E'\right)}{(1+\nu)\left(1-\nu-2E\nu'^2/E'\right)}, \qquad c_{013} = \frac{E\nu'}{\left(1-\nu-2E\nu'^2/E'\right)}, \qquad c_{044} = G' \\
c_{033} &= \frac{E'(1-\nu)}{\left(1-\nu-2E\nu'^2/E'\right)}, \qquad c_{066} = \frac{E}{2(1+\nu)} = G, \quad c_{012} = c_{011} - 2c_{066}.
\end{aligned}
\tag{86}
$$

The materials in Table 1 are selected in such a way that the ratio E'/E varies over a wide range. Since, we are concerning the vertical force and movements, this ratio may be the best parameter to portray the main effect of degree of anisotropy.

Before presenting a parametric study for the wave propagation characteristics of non-homogeneous transversely isotropic materials, it is essential to demonstrate to some extent that the mixed boundary value problem stated in equation (3) to (8) has been satisfied numerically. At the interface of two joined half-spaces, the results of radial and vertical

displacements of exponentially graded transversely isotropic materials have been depicted in Figs. 3 and 4 for the fixed value of the frequency of vibration. As it can be seen, the prescribed displacements, equations (3) to (4), have been successfully imposed at the location of plate area, but since no displacement boundary condition has been held for penny-shaped crack, the variation of displacements on the other face of the crack is consistent with the vertical movement of plate. The displacements at the upper and the lower half-spaces are met each other just at the edge of the plate, causing severe variation for displacements around the boundary of the plate. Similarly, the stress components of materials are plotted in Figs. 5 and 6, which show the singular nature of stress functions at the edge of both penny-shaped crack and plate. The continuity of displacements and stresses is also completely valid after the plate/crack position.

The influence of non-homogeneity of the material on the dynamic behavior of transversely isotropic full-space has been illustrated in Figs. 7a and 7b on the axis of symmetric of the materials. At the position of the plate/crack discontinuity, a finite jump in displacements of the materials is evident. The magnitude of the function of vertical displacement, as demonstrated in Fig. 7, has been mitigated by increasing the non-homogeneity of the material and vanished at a place far from plate/crack position. The dynamic load-displacement relationship, the impedance functions, of the rigid plate in vertical direction is an important physical quantity that can be defined as

$$K_{VV}(\omega_0) = \frac{F(\omega_0)}{C_{440} a \Delta}, \tag{87}$$

where

$$\omega_0 = a\omega\sqrt{\frac{\rho}{c_{440}}}. \tag{88}$$

Figures 8 to 11 depict the effect of inhomogeneity and anisotropy of the material on both the trend and the magnitude of impedance functions. Figure 8 shows the impedance function for a rigid inclusion surrounded by the crack embedded in a homogeneous full-space material (i.e. the non-homogeneity parameter is held zero). As expected, a wavy behavior has been observed from the figures as the non-dimensional frequency of vibration is increased. It is evident that the magnitude of impedance function will increase if the value of E' of the material increases, but the shapes of impedance functions stay nearly intact. On the other hand, as E of the material increases, both the shape and magnitude of the impedance function vary with frequency.

Before discussing the effect of non-homogeneity of the material on the impedance functions, it is essential to check the possibility of the condition in which the rigid plate attached to both sides of upper and lower half-spaces. This situation may occur as a result of large vertical deformation of the plate through dynamic action in conjunction with the change in the loading direction. Alternatively, the continuity of the contact conditions at the penny-shaped crack might be violated under severe loading. In this case, if the radius of the crack is substantially increased in such a way that it asymptotically approaches infinity, the problem identical to the vibration of the inclusion on the half-space would result. The analytical treatment for the stated physical problems needs separate studies which are available in the literature for certain cases. By assuming a relaxed condition that leads to an excellent approximation of the bonded one, similar problems have been investigated in [39-40] without material defects in full-space or half-space. Those results are suitable for comparison since, geometrically, they can be considered as the specific case of present study. Thus, the results of [39-40] are presented in Fig. 9 together with results of our study, the latter being extracted and calculated for the Case II introduced in Table 1. As can be seen, the trend of impedance functions for this study in both real and imaginary parts are different from those of other cases. Besides, in comparing with other cases, the results of the present study show a wavy behavior, which can be attributed from the scattering phenomena generated by material defects, however, the range of oscillation is low in comparison with the solutions presented for upper and lower bounds.

The influences of material inhomogeneity on the dynamic stiffness of the embedded inclusion are illustrated in the Figs. 10 and 11. For increasing the material inhomogeneity, the value of impedance function gradually grows since transversely isotropic materials tend to be further stiffer by increasing the inhomogeneity parameter and, as a result, the frequency-dependent behavior of the material, has been rapidly decayed. An interesting point of Fig. 10 is that the imaginary part of the impedance function approaches zero below a so-called cut-off frequency. Below this frequency, the wave propagation does not occur and the impedance function is close to the static value. This effect similarly is also observed in the problem of vibration of a plate made of an inhomogeneous isotropic material [29] and, with reference to the numerical result of this paper (see Fig. 10), the material anisotropy has no influence on the onset of this phenomenon and they have just related to the parameter of non-homogeneity of the material. This statement is further confirmed by numerical results presented in Fig. 11, where the impedance function of the rigid plate is derived for different inhomogeneous materials. It is evident that the asymptotic behavior of the imaginary part of the impedance function tends to a fixed value regardless of any chosen parameter for the material inhomogeneity.

7. Conclusion

Mixed boundary value problem associated with the vertical vibration of a rigid circular plate partially in contact with an inhomogeneous transversely isotropic full-space has been formulated with the aid of a newly developed displacement potential method. By utilizing Hankel integral transforms and defining auxiliary functions, the problem is converted to the solution of a set of coupled integral equations, which are both analytically and numerically examined to reveal a mechanical characteristic of the system. The closed-form solution for vertical movement of the plate in a homogeneous transversely isotropic material is found in explicit form, which was observed that the contact load distribution possess a kind of oscillatory singularity at the region near the edge of the plate. The analytical solutions presented in the paper are completely in agreement with the existing formulation previously reported in the literature for the special case of homogeneous isotropic material.

To numerically assess the forced vibration of the plate in full-space material, the method of discrete collocation-based on the expansion of auxiliary functions is employed. It is shown that imposing the boundary condition may cause severe variation of elastic fields near the edge of both plate and penny-shaped crack. Furthermore, the inhomogeneity of the material has been shown to have a major contribution to fast decay of displacement function with depth. From the parametric study of the material properties, Young's modulus in the plane of isotropy has a major role in the frequency-dependent response of materials in terms of computed impedance functions. However, the dynamic behavior of a functionally graded material will be less dependent on the frequency of vibration if the material inhomogeneity increases. It is observed that, below certain fixed frequencies of the vibration, the imaginary part of impedance functions approaches zero. The mathematical formulation presented in this paper can be readily extended to the problem of vibration of the plate in an inhomogeneous transversely isotropic material loaded in different directions.

Acknowledgement. The authors wish to thank Prof. A.P.S. Selvadurai (McGill University) and Prof. M. Eskandari-Ghadi (University of Tehran) for their valuable comments during the preparation of the manuscript. This work has partially been supported by the NSF under grant IIP-1362146 (I/UCRC: Novel High Voltage/Temperature Materials and Structures).

Appendix A

A list of mathematical identities used in the paper is summarized in this section [36].

$$\int_0^\infty J_\nu(r\xi)\sin(s\xi)d\xi=\begin{cases}\dfrac{\sin\left(\nu\arcsin(s/r)\right)}{\sqrt{r^2-s^2}}, & s<r\\ \infty \text{ or } 0, & s=r\\ \dfrac{r^\nu\cos(\nu\pi/2)}{\sqrt{s^2-r^2}(s+\sqrt{s^2-r^2})^\nu}, & s>r\end{cases} \tag{A1}$$

$$\int_0^\infty J_\nu(r\xi)\cos(s\xi)d\xi=\begin{cases}\dfrac{\cos\left(\nu\arcsin(s/r)\right)}{\sqrt{r^2-s^2}}, & s<r\\ \infty \text{ or } 0, & s=r\\ \dfrac{-r^\nu\sin(\nu\pi/2)}{\sqrt{s^2-r^2}\left(s+\sqrt{s^2-r^2}\right)^\nu}, & s>r\end{cases} \tag{A2}$$

$$J_1(r\xi)=-\frac{d}{\xi dr}\left(J_0(r\xi)\right) \tag{A3}$$

$$J_0(r\xi)=\frac{d}{r\xi dr}\left(rJ_1(r\xi)\right) \tag{A4}$$

$$H(a,\theta,\xi)=\int_{-a}^{a}\left(\frac{a-s}{a+s}\right)^{i\theta}e^{-is\xi}ds=2a\beta(1-i\theta,1+i\theta)e^{i\xi a}{}_1F_1(1-i\theta;2;-2i\xi a). \tag{A5}$$

In the above identity, $\beta(a,b)=\int_0^1 t^{a-1}(1-t)^{b-1}dt$ is the Beta function and $F_1(a;b;c)$ is the confluent hypergeometric function, see Appendix A in [37].

Appendix B

The numerical process for determining the auxiliary functions is presented here. Since the orthogonal Chebyshev polynomials have been restricted to the finite interval (-1,1), it is normalized to the interval of integral equations by introducing

$$s=a\bar{s};\quad t=a\bar{t}; \tag{B1}$$

Thus, we take the following expansion for auxiliary functions

$$A(\bar{s}) = w(\bar{s})\sum_{i=0}^{n} a_i T_i(\bar{s}),\ B(\bar{s}) = w(\bar{s})\sum_{i=0}^{n} b_i T_i(\bar{s}),$$
$$\alpha(\bar{s}) = w(\bar{s})\sum_{i=0}^{n} c_i T_i(\bar{s}),\ \beta(\bar{s}) = w(\bar{s})\sum_{i=0}^{n} d_i T_i(\bar{s}), \tag{B2}$$

where $w(\bar{s})$ is weighting function equal to $1/\sqrt{1-\bar{s}^2}$ and $T_i(\bar{s})$ is Chebyshev polynomial of the first order and defined as

$$T_i(\bar{s}) = Cos(i\ Arc\cos(\bar{s})). \tag{B3}$$

By substituting (B2) in equation (53) to (56) and taking the advantage of the identity [38]

$$\int_{-1}^{1} \frac{w(\bar{t})T_i(\bar{t})}{\bar{t}-\bar{s}}\,d\bar{t} = \pi U_{i-1}(\bar{s}), \tag{B4}$$

where $U_{i-1}(\bar{s})$ is Chebyshev polynomial of the second order, which is defined as

$$U_{i-1}(\bar{s}) = \frac{sin(\mathrm{i}\ cos^{-1}(\bar{s}))}{sin(cos^{-1}(\bar{s}))}. \tag{B5}$$

we have

$$-L_{11}\sum_{i=0}^{n} c_i U_{i-1}(\bar{s}) + L_{12}\sum_{i=0}^{n} d_i (w(\bar{s})T_i(\bar{s}) + K_{12}^{i}(\bar{s})) + L_{13}\sum_{i=0}^{n} b_i (w(\bar{s})T_i(\bar{s}) + K_{13}^{i}(\bar{s})) = 0, \tag{B6}$$

$$L_{21}\sum_{i=0}^{n} c_i (w(\bar{s})T_i(\bar{s}) + K_{21}^{i}(\bar{s})) + L_{22}\sum_{i=0}^{n} d_i U_{i-1}(\bar{s}) + L_{24}\sum_{i=0}^{n} a_i (w(\bar{s})T_i(\bar{s}) + K_{24}^{i}(\bar{s})) = \frac{2}{\pi}\Delta, \tag{B7}$$

$$L_{31}\sum_{i=0}^{n} c_i (w(\bar{s})T_i(\bar{s}) + K_{31}^{i}(\bar{s})) + L_{33}\sum_{i=0}^{n} b_i U_{i-1}(\bar{s}) + L_{34}\sum_{i=0}^{n} a_i (w(\bar{s})T_i(\bar{s}) + K_{34}^{i}(\bar{s})) = -\frac{2}{\pi}C, \tag{B8}$$

$$L_{42}\sum_{i=0}^{n} d_i (w(\bar{s})T_i(\bar{s}) + K_{42}^{i}(\bar{s})) + L_{43}\sum_{i=0}^{n} b_i (w(\bar{s})T_i(\bar{s}) + K_{43}^{i}(\bar{s})) - L_{44}\sum_{i=0}^{n} a_i U_{i-1}(\bar{s}) = 0, \tag{B9}$$

where

$$K_{pq}^{i}(\bar{s}) = a\int_{-1}^{1} w(\bar{t})k_{pq}(\bar{t},\bar{s})T_i(\bar{t})d\bar{t}\,. \tag{B10}$$

Considering the kernel given in (B10), it is reasonable to employ a Chebyshev–Gauss quadrature rule for evaluation of integrals

$$K_{pq}^{i}(\bar{s}) = a\int_{-1}^{1} w(\bar{t})k_{pq}(\bar{t},\bar{s})\,T_i(t)dt = a\sum_{j=1}^{m} W_j\, k_{pq}(\bar{t_j},\bar{s})\,T_i(\bar{t_j}), \tag{B11}$$

where

$$W_j = \frac{\pi}{m}, \qquad \bar{t_j} = cos\,\frac{(2j-1)\pi}{2m}. \tag{B12}$$

The consistency condition expressed in equation (46) should also be included, implying $c_0 = 0$ which gives an extra equation. Then, constant C plus unknown coefficients of B2 can be obtained using this extra equation, $c_0 = 0$, alongside with the system of coupled equations B6 to B9.

References

[1]. C.B. Crouse, B. Hushmand, J.E. Luco, H.L. Wong, Foundation impedance functions: theory versus experiment. *ASCE J. Geotech. Eng*. **116**(3), 432-449 (1990).

[2]. R. Pak, J.C. Ashlock., S. Kurahashi, M. Soudkhah, Physical characteristics of dynamic vertical–horizontal-rocking response of surface foundations on cohesionless soils. *Géotechnique* **61**(8), 687 (2011).

[3]. G. Gazetas, Analysis of machine foundation vibrations: state of the art. *Soil Dyn. Earthquake Eng*. **2**(1), 2-42 (1983).

[4]. J.P. Wolf, Consistent lumped-parameter models for unbounded soil: Physical representation. *Earthq. Eng. Struct. Dyn*. **20**(1), 11-32 (1991).

[5]. W.H. Wu, C.Y. Chen, Simplified Soil-Structure Interaction Analysis Using Efficient Lumped-Parameter Models for Soil. *Soils Found*. **42**(6), 41-52 (2002).

[6]. B.W. Byrne, G.T. Houlsby, Foundations for offshore wind turbines. *Philos. Trans. Roy. Soc. A* **361**(1813), 2909-2930 (2003).

[7]. D. Lombardi, S. Bhattacharya, D.M. Wood, Dynamic soil–structure interaction of monopile supported wind turbines in cohesive soil. *Soil Dyn. Earthquake Eng*. **49**, 165-180 (2013).

[8]. S. Malhotra, Design and construction considerations for offshore wind turbine foundations. In *ASME 26th International Conference on Offshore Mechanics and Arctic Engineering*. American Society of Mechanical Engineers (2007).

[9]. D.S. Jeng, Soil response in cross-anisotropic seabed due to standing waves. *J. Geotech. Geoenviron. Eng*. **123**(1), 9-19 (1997).

[10]. M. R. Naeeni, M. Eskandari-Ghadi, A.A. Ardalan, R.Y.S. Pak, M. Rahimian, Y. Hayati. Coupled thermoviscoelastodynamic Green's functions for bi-material half-space. *ZAMM* **95**(3), 260-282 (2015).

[11]. R.S. Kourkoulis, P.C. Lekkakis, F.M. Gelagoti, A.M. Kaynia, Suction caisson foundations for offshore wind turbines subjected to wave and earthquake loading: effect of soil-foundation interface. *Géotechnique* **64**(3), 171-185 (2014).

[12]. V. Zania, Natural vibration frequency and damping of slender structures founded on monopiles. *Soil Dyn. Earthquake Eng*. **59**, 8-20 (2014).

[13]. F. Delale, F. Erdogan, The crack problem for a non-homogeneous plane. *ASME J. Appl. Mech.* **50**(3), 609-614 (1983).

[14]. P.S. Dineva, G.D. Manolis, Scattering of seismic waves by cracks in multi-layered geological regions: I. Mechanical model. *Soil Dyn. Earthquake Eng.* **21**(7), 615-625 (2001).

[15]. P.S. Dineva, G.D. Manolis, Scattering of seismic waves by cracks in multi-layered geological regions: II. Numerical results. *Soil Dyn. Earthquake Eng*. **21**(7), 627-641 (2001).

[16]. Y.S. Chan, G.H. Paulino, AC. Fannjiang, The crack problem for non-homogeneous materials under anti plane shear loading—a displacement based formulation. *Int. J. Solids Struct*. **38**(17), 2989-3005 (2001).

[17]. D.L. Clements, An antiplane crack between bonded dissimilar continuously inhomogeneous isotropic elastic materials. *Quart. J. Mech. Appl. Math*. **66**(3), 333-349 (2013).

[18]. R. Babaei, S.A. Lukasiewicz. Fracture in Functionally Gradient Materials Subjected to the Time-Dependent Anti-Plane Shear Load. *ZAMM* **78**(6), 383-390 (1998).

[19]. A.P.S. Selvadurai, The penny-shaped crack at a bonded plane with localized elastic non-homogeneity. *Eur. J. Mech. A. Solids* **19**(3), 525-534 (2000).

[20]. J. Vrbik, B. M. Singh, J. Rokne, R.S. Dhaliwal, On the expansion of a penny-shaped crack by a rigid circular disc inclusion in a thick plate. *ZAMM* **84**(8), 538-550 (2004).
[21]. L.M. Keer, Mixed boundary value problems for a penny-shaped cut. *J. Elast*. **5**(2), 89-98 (1975).
[22]. A.P.S. Selvadurai, A contact problem for a smooth rigid disc inclusion in a penny-shaped crack. *Z. Angew. Math. Phys*. **45**(1), 166-173 (1994).
[23]. N.I. Muskhelishvili, *Some Basic Problems of the Mathematical Theory of Elasticity* (No. 1). Springer. (1977)
[24]. R. Ballarini, A certain mixed boundary value problem for a bimaterial interface. *Int. J. Solids Struct*. **32**(3), 279-289 (1995).
[25]. G.M.L. Gladwell, On inclusions at a bi-material elastic interface. *J. Elast.* **54**(1), 27-41 (1999).
[26]. A.O. Awojobi, Vertical vibration of a rigid circular foundation on Gibson soil. *Géotechnique* **22**(2), 333-343 (1972).
[27]. A.O. Awojobi, Vibration of rigid bodies on non-homogeneous semi-infinite elastic media. *Quart. J. Mech. Appl. Math*. **26**(4), 483-498 (1973).
[28]. R.Y.S Pak, A.T. Gobert, Forced vertical vibration of rigid discs with arbitrary embedment. *ASCE J. Eng. Mech*. **117**(11), 2527-2548 (1991).
[29]. B.B. Guzina, R.Y.S. Pak. Vertical vibration of a circular footing on a linear-wave-velocity half-space. *Géotechnique* **48**(2), 159-168 (1998).
[30]. M. Eskandari-Ghadi, A. Ardeshir-Behrestaghi, Forced vertical vibration of rigid circular disc buried in an arbitrary depth of a transversely isotropic half space. *Soil Dyn. Earthquake Eng*. **30**(7), 547-560 (2010).
[31]. M. Eskandari-Ghadi, A. Mirzapour, A. Ardeshir-Behrestaghi, Rocking vibration of rigid circular disc in a transversely isotropic full-space, *Int. J. Numer. Anal. Methods Geomech*. **35**(14), 1587–1603(2011).
[32]. M. Eskandari-Ghadi, A. Ardeshir-Behrestaghi, B. Navayi Neya, Mathematical analysis for an axissymmetric disc-shaped crack in transversely isotropic half-space. *Int. J. Mech. Sci.* **68**,171-179 (2013).
[33]. B.B. Guzina, R.Y.S Pak, On the analysis of wave motions in a multi-layered solid. *Quart. J. Mech. Appl. Math*. **54**(1), 13-37 (2001).
[34]. M. Eskandari-Ghadi, A. Amiri-Hezaveh, Wave propagations in exponentially graded transversely isotropic half-space with potential function method. *Mech. Mater*. **68**,275-292 (2014).
[35]. R.Y.S Pak, Asymmetric wave propagation in an elastic half space by a method of potentials. *ASME J. Appl. Mech***. 54**(1), 121–126 (1987).
[36]. I.S. Gradshteyn, I.M. Ryzhik. *Table of Integrals, Series, and Products*. Academic Press (2007)

[37]. I.N. Sneddon, *Fourier Transforms*, McGraw Hill Book Co., New York (1951)

[38]. F. Erdogan, K. Arin, Penny-shaped interface crack between an elastic layer and half space. *Int. J. Eng. Sci*. **10**(2), 115-125(1972).

[39]. A.R. Hajimohammadi, A. Khojasteh, M. Rahimian, R.Y.S Pak, Vertical vibration of a rigid circular disc at the interface of a transversely isotropic bi-material. *Int. J. Solids Struct*. **50**(18), 2772-2780 (2013).

[40]. M. Eskandari-Ghadi, M. Fallahi, A. Ardeshir-Behrestaghi, Forced vertical vibration of rigid circular disc on a transversely isotropic half-space. *ASCE J. Eng. Mech*. **136**(7), 913-922 (2009).

Figure Captions

Fig. 1. Wind turbine foundation subjected to dynamic loading.

Fig. 2. A rigid circular inclusion inside an exponentially graded transversely isotrop*ic* full-space.

Fig. 3. Radial displacement at the interface of two half-spaces in an exponentially graded transversely isotropic material $(\omega_0 = 3.0,\ \beta_s = 0.25)$; Mat I.

Fig. 4. Vertical displacement at the interface of two half-spaces in a continuously inhomogeneous transversely isotropic material $(\omega_0 = 3.0,\ \beta_s = 0.25)$; Mat I.

Fig. 5. Shear stress in a non-homogeneous transversely isotropic material at the interface of two half-spaces $(\omega_0 = 3.0,\ \beta_s = 0.25)$; Mat I.

Fig. 6. Normal stress in non-homogeneous transversely isotropic material at the interface of two half-spaces $(\omega_0 = 3.0,\ \beta_s = 0.25)$; Mat I.

Fig. 7a. Vertical displacement along the z direction for different non-homogeneous transversely isotropic materials. Real part ($\omega_0 = 3.0$); Mat III.

Fig. 7b. Vertical displacement along the z direction for different non-homogeneous transversely isotropic materials. Imaginary part ($\omega_0 = 3.0$); Mat III.

Fig. 8a. Impedance functions of a rigid circular inclusion for different homogeneous transversely isotropic materials. Real part ($\beta_s = 0$)

Fig. 8b. Impedance functions of a rigid circular inclusion for different homogeneous transversely isotropic materials. Imaginary part ($\beta_s = 0$)

Fig. 9a. Impedance function of a rigid disc weakened by a penny-shaped crack compared with similar functions for a disc vibrated on half-space or embedded in the full-space material. Real part.

Fig. 9b. Impedance function of a rigid disc weakened by a penny-shaped crack compared with similar functions for a disc vibrated on half-space or embedded in the full-space material. Imaginary part.

Fig. 10. Impedance functions of a rigid circular inclusion for different non-homogeneous transversely isotropic materials ($\beta_s = 0.25$).

Fig. 11. The influence of non-homogeneity of the materials on impedance functions of a rigid circular inclusion (Mat II).

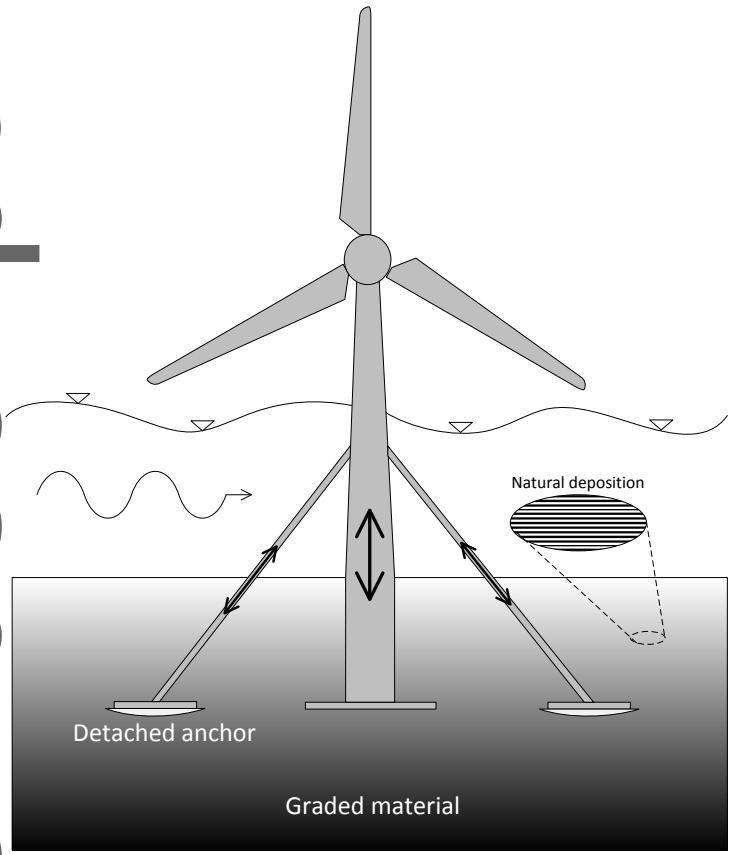

Fig 1. Wind turbine foundation subjected to dynamic loading.

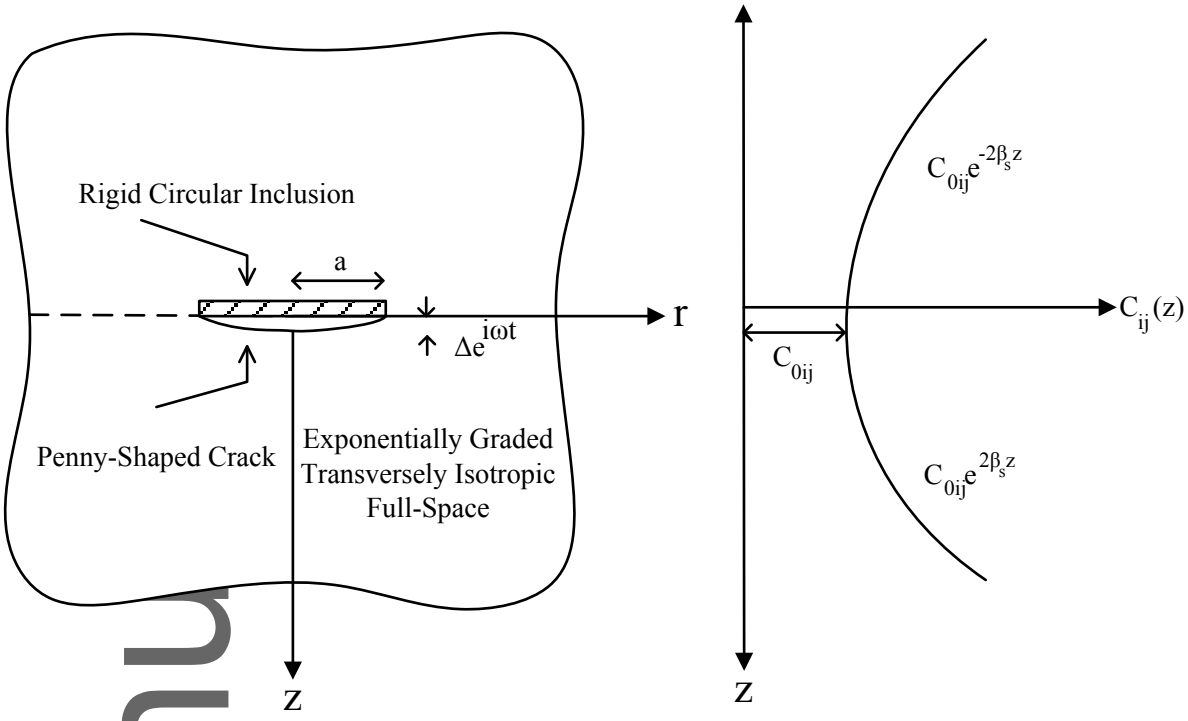

Fig 2. A rigid circular inclusion inside an exponentially graded transversely isotropic full-space.

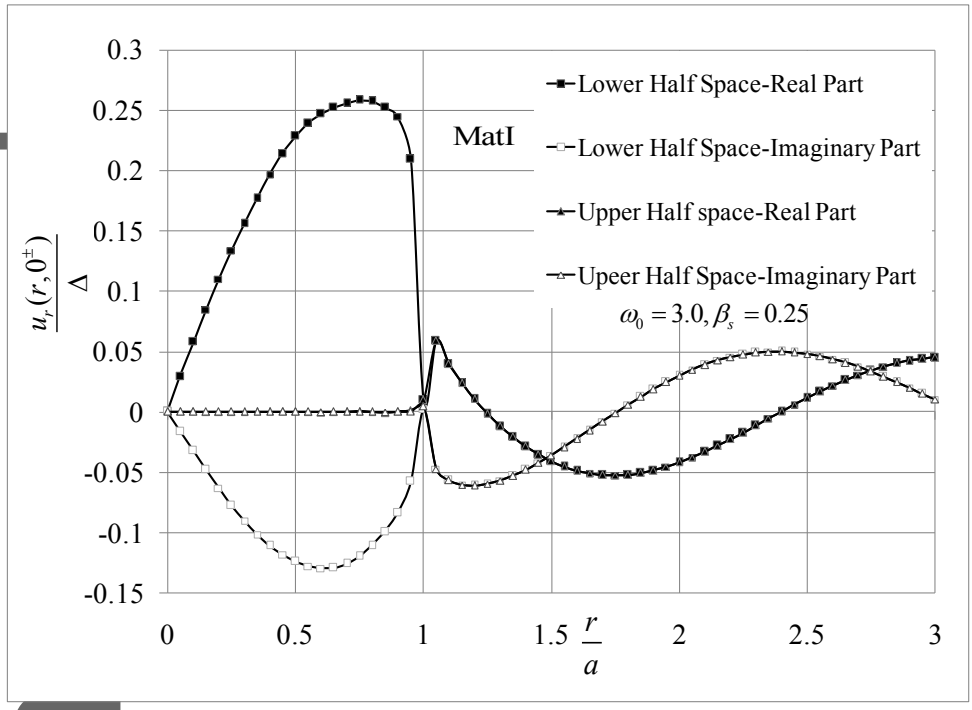

Fig 3. Radial displacement at the interface of two half-spaces in exponentially graded transversely isotropic material $(\omega_0 = 3.0,\ \beta_s = 0.25)$; Mat I.

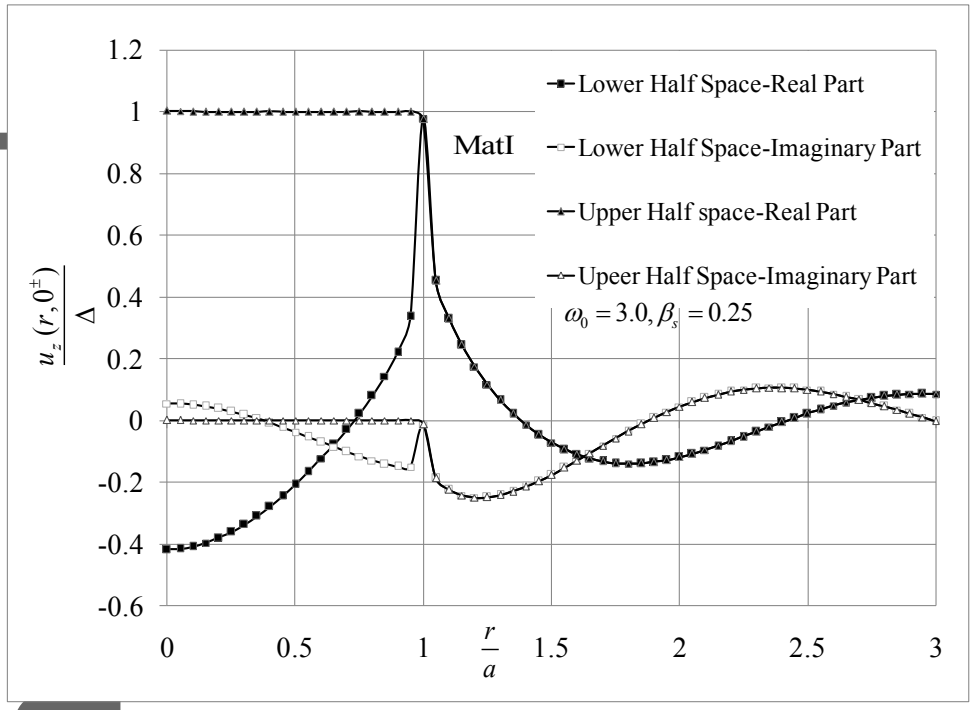

Fig.4. Vertical displacement at the interface of two half-spaces in a continuously inhomogeneous transversely isotropic material ($\omega_0 = 3.0,\ \beta_s = 0.25$); Mat I.

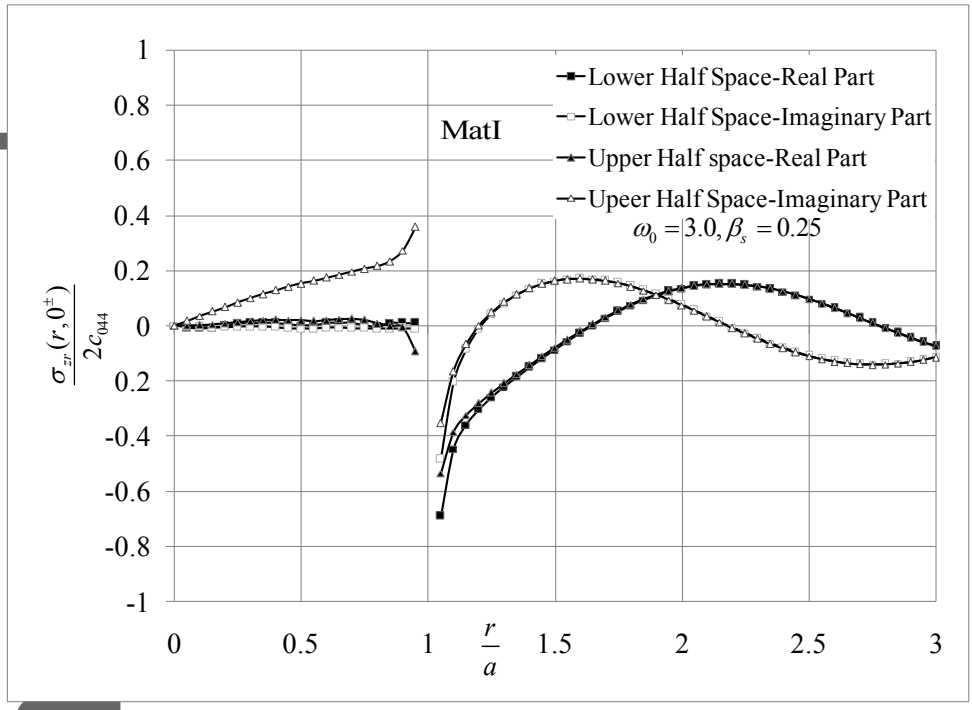

Fig 5. Shear stress in a non-homogeneous transversely isotropic material at the interface of two half spaces $(\omega_0 = 3.0,\ \beta_s = 0.25)$; Mat I.

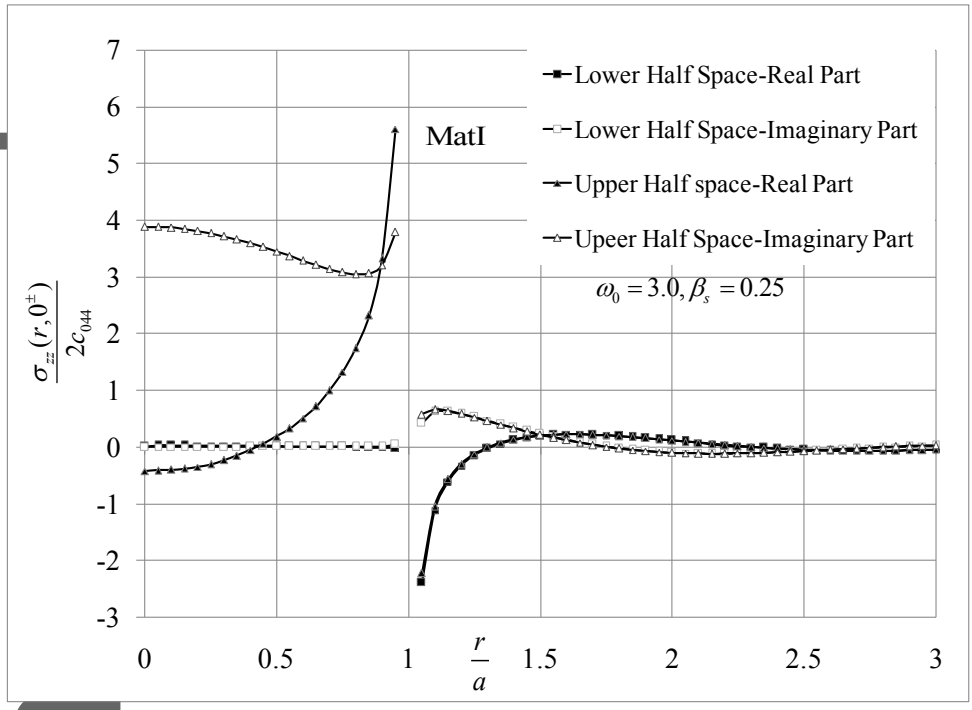

Fig 6. Normal stress in non-homogeneous transversely isotropic material at the interface of two half spaces $(\omega_0 = 3.0,\ \beta_s = 0.25)$; Mat I.

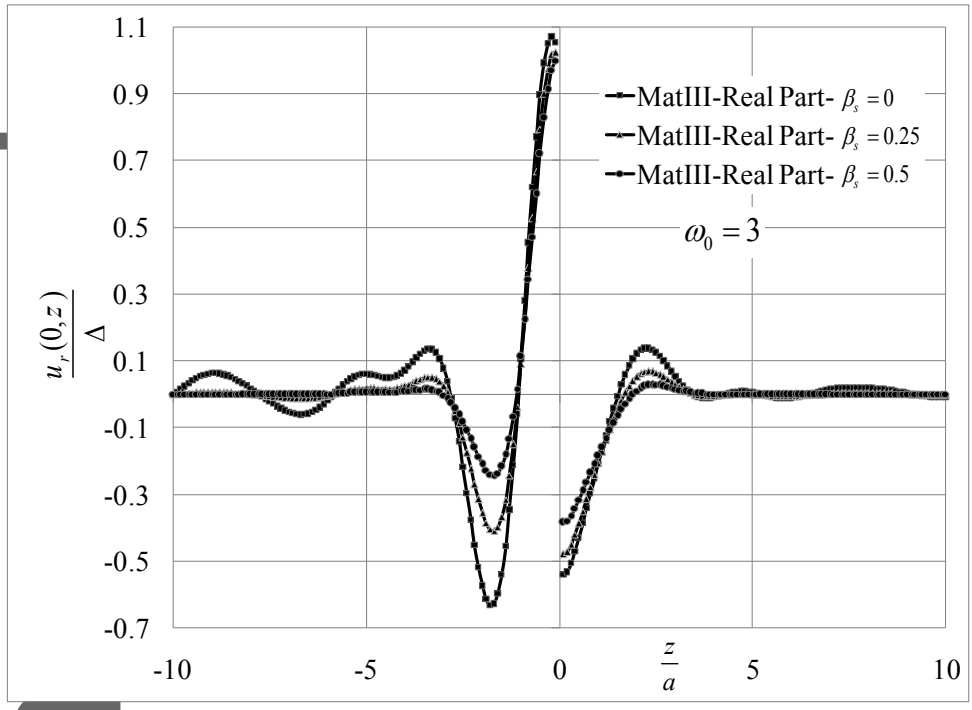

Fig 7a. Vertical displacement along the z direction for different non-homogeneous transversely isotropic materials. Real part ($\omega_0 = 3.0$; Mat III).

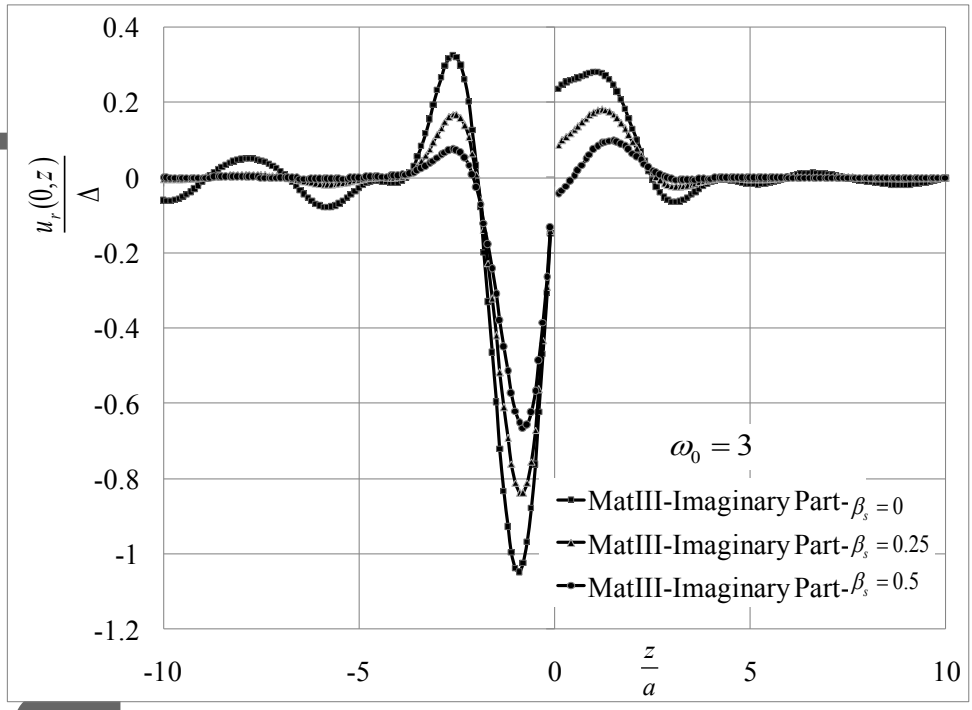

Fig 7b. Vertical displacement along the z direction for different non-homogeneous transversely isotropic materials. Imaginary part ($\omega_0 = 3.0$; Mat III).

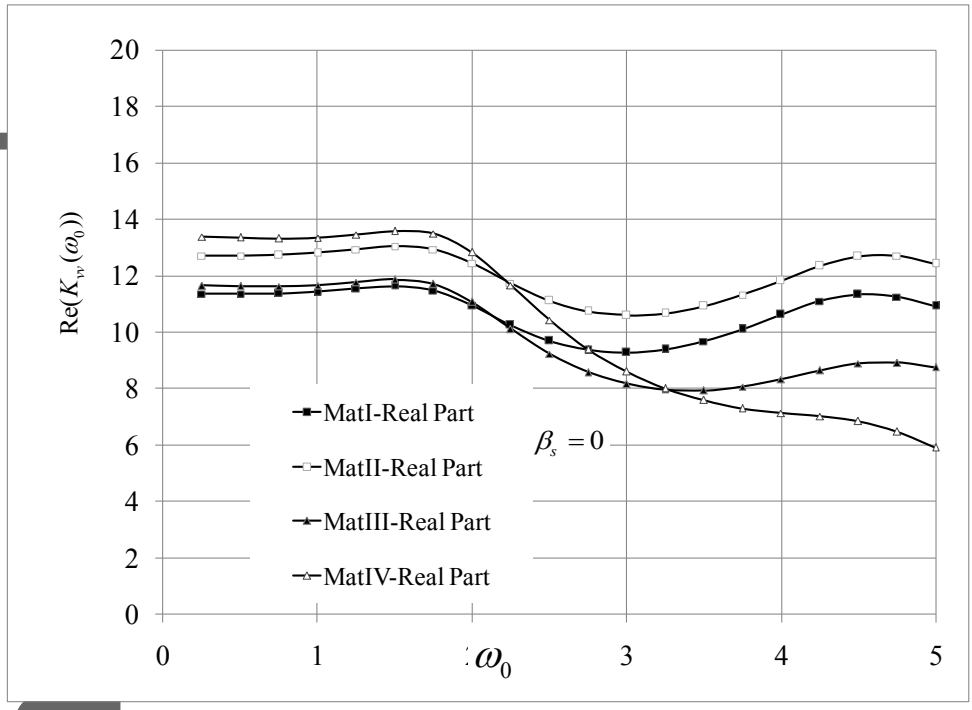

Fig 8a. Impedance functions of a rigid circular inclusion for different homogeneous transversely isotropic materials b) Real part ($\beta_s = 0$)

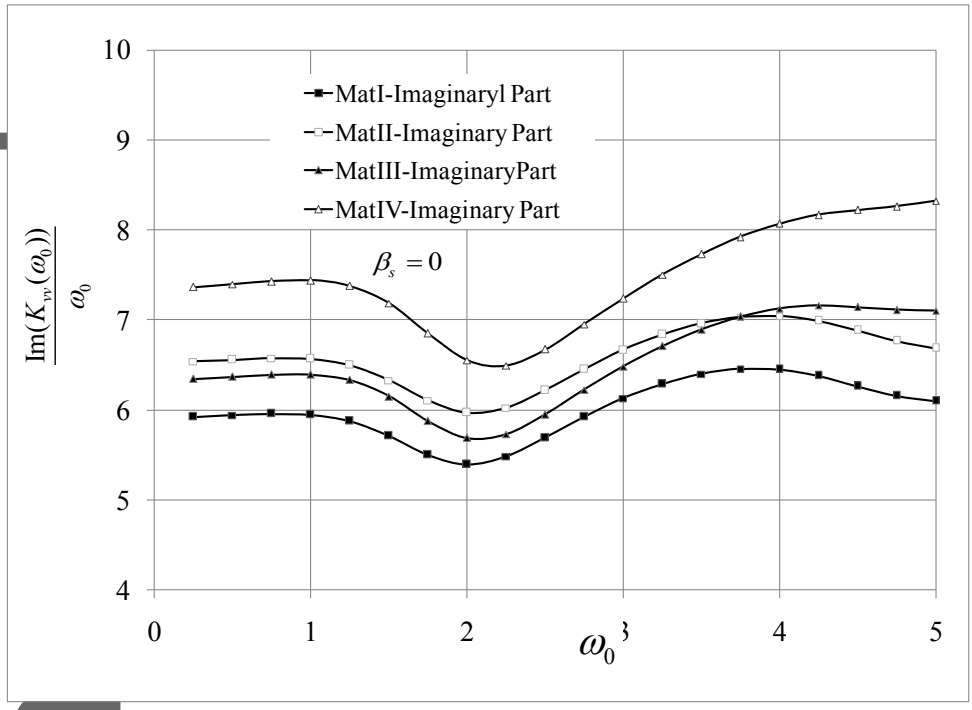

Fig 8b. Impedance functions of a rigid circular inclusion for different homogeneous transversely isotropic materials. Imaginary part ($\beta_s = 0$).

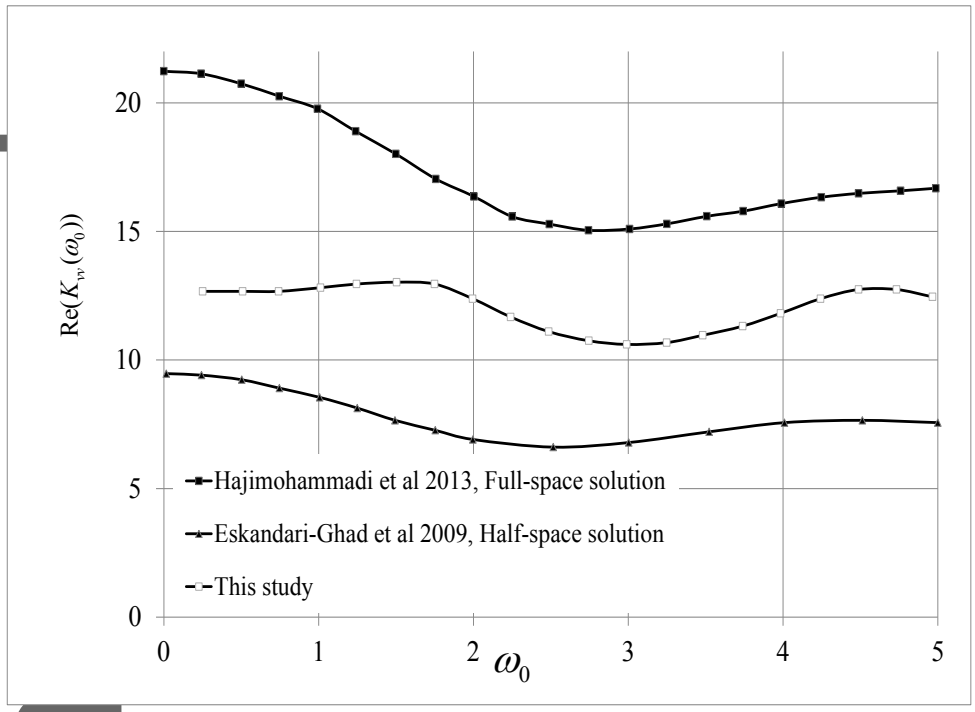

Fig 9a. Impedance function of a rigid disc weakened by a penny-shaped crack compared with similar functions for a disc vibrated on half-space or embedded in the full-space material. Real part.

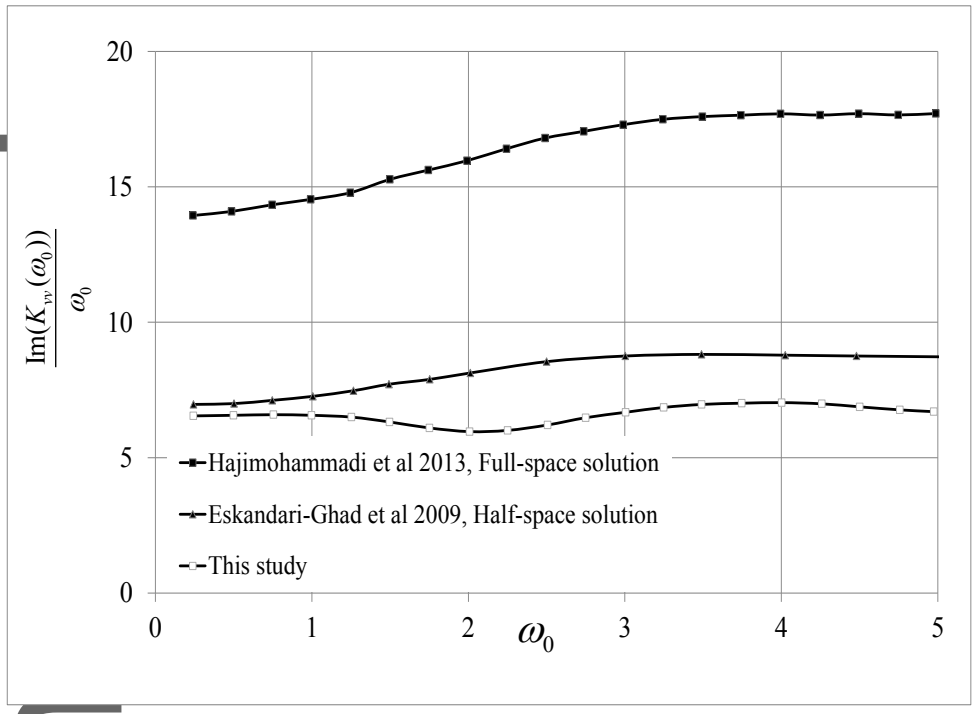

Fig 9b. Impedance function of a rigid disc weakened by a penny-shaped crack compared with similar functions for a disc vibrated on half-space or embedded in the full-space material. Imaginary part.

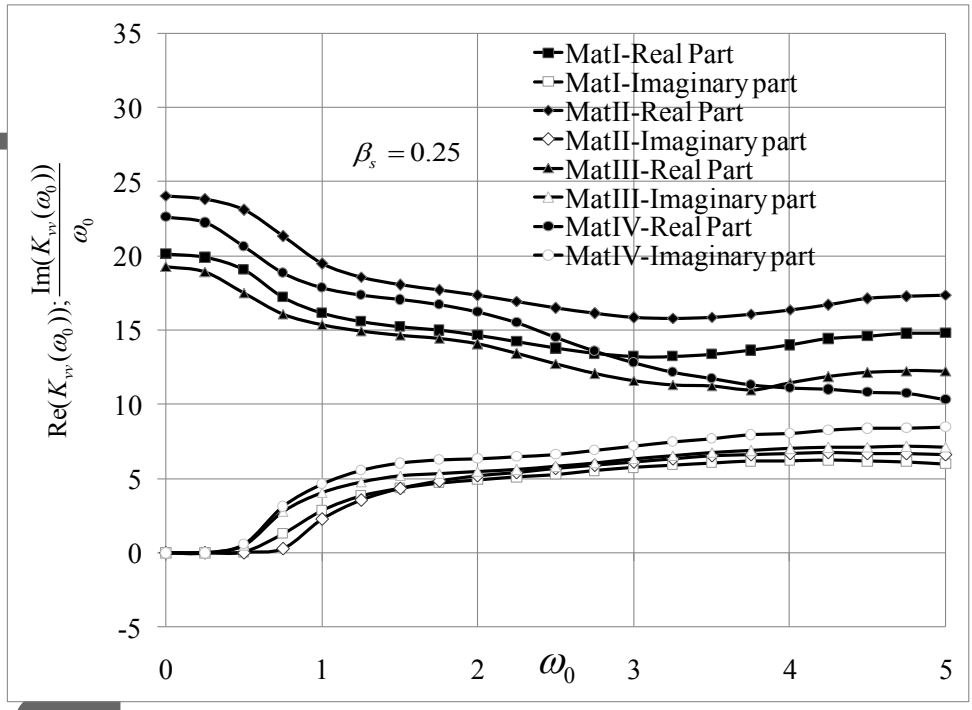

Fig 10. Impedance functions of a rigid circular inclusion for different non-homogeneous transversely isotropic materials ($\beta_s = 0.25$).

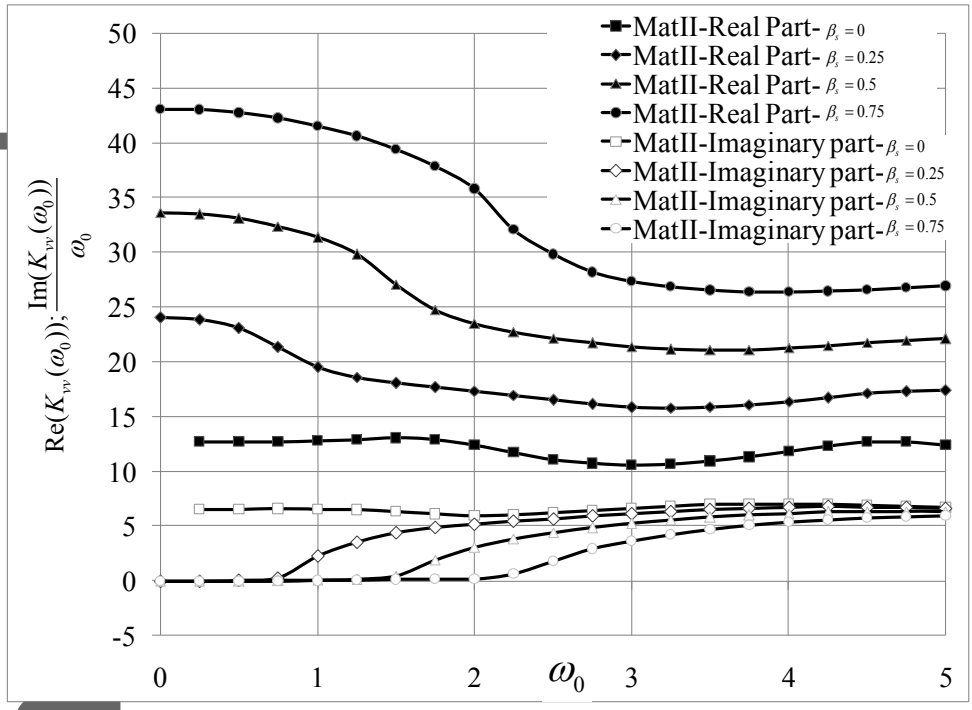

Fig 11. The influence of non-homogeneity of the materials on impedance functions of a rigid circular inclusion (Mat II).

Table 1. Synthetic material engineering constants

Material Properties	Case I	Case II	Case III	Case IV
E'	100000	150000	50000	50000
E'	2	3	$1/3$	$1/3$
G	20000	20000	60000	60000
For all cases: G'=20000 N/mm^2, $\nu = \nu' = 0.25$				